

Manifold Optimization for High Accuracy Spatial Location Estimation Using Ultrasound Waves

Mohammed H. AlSharif, *Student Member, IEEE*, Ahmed Douik, *Student Member, IEEE*,
Mohanad Ahmed, Tareq Y. Al-Naffouri, *Senior Member, IEEE*, and Babak Hassibi, *Member, IEEE*

Abstract—This paper designs a high accuracy spatial location estimation method using ultrasound waves by exploiting the fixed geometry of the transmitters. Assuming an equilateral triangle antenna configuration, where three antennas are placed as the vertices of an equilateral triangle, the spatial location problem can be formulated as a non-convex optimization problem whose interior is shown to admit a Riemannian manifold structure. The investigation of the geometry of the newly introduced manifold, i.e. the manifold of all equilateral triangles in \mathbb{R}^3 , allows the design of highly efficient optimization algorithms. Simulation results are presented to compare the performance of the proposed approach against popular methods from the literature. The results suggest that the proposed Riemannian-based methods outperform the state-of-the-art methods. Furthermore, the proposed Riemannian methods require much smaller computation time as compared with popular generic non-convex approaches.

Index Terms—Spatial location estimation, ultrasound waves, fixed transmitters geometry, Riemannian manifold optimization.

I. INTRODUCTION

WITH the rapidly increasing number of smartphones and the proliferation of the Internet of Things (IoT), location-based services gained an increased interest in the last decade [1]. These services range from outdoor localization, e.g., for navigation purposes, to accurate indoor pinpointing for applications such as robot steering, surveillance, video gaming, and virtual reality [2]. While outdoor localization is universally solved by the Global Navigation Satellite System (GNSS), such a system is not feasible indoors. As such, indoor localization systems have been implemented using various competing technologies, including ultrasound waves [3], radio-frequency [4], infrared radiation [5], and laser signals [6].

Light-based localization systems, i.e., radio, infrared, and laser signals, suffer from a low accuracy or a high hardware cost. Indeed, due to the high speed of light and without precise and costly synchronization, small timing errors result in significant localization errors [7]. As a result, localization systems based on WiFi or Bluetooth technologies have low accuracy and require pre-calibration [8]. Similarly, while radio-based

approaches, utilizing the time of flight¹ (ToF) estimation, do not require pre-calibration, these systems depend on an exact synchronization. Finally, laser and infrared-based localization devices are complicated and expensive to build and maintain [9]. This paper considers ultrasound-based localization methods [10] for their low cost and high accuracy, which is enabled by the relatively low speed of sound [11].

Besides the effects of the employed technology, the accuracy of indoor localization systems primarily depends on the optimization algorithms utilized in the design of those systems, e.g., see [12], [13], and references therein. For example, a simple approach consists of estimating the Received Signal Strength (RSS). While popular, the RSS-based methods suffer from poor localization accuracy due to multipath fading and temporal dynamics [14]. Alternatively, the Angle of Arrival (AoA) can be exploited to design high accuracy systems for close-range location estimation. However, its performance significantly degrades as the distance between the transmitter and the receiver increases. This accuracy deterioration is a consequence of the fact that a tiny error in the estimated angle results in a massive failure in the estimated position [15].

The previously mentioned ToF-based approach represents an attractive alternative for its simplicity. Still, a small perturbation in the estimated ToF can result in a significant deviation in the expected location, especially under an unfavorable geometry [16]. To circumvent the aforementioned limitation, this manuscript uses multiple transmitters and considers exploiting their geometry in the estimation process. The resulting transmitter diversity not only significantly improves the accuracy of the estimated location but also provides the 3D orientation of the device.

In particular, this paper considers a target with three transmitters that are placed on an equilateral triangle and utilizes a set of four receivers, known as beacons, to estimate the 3D location and orientation of the target accurately. The positions of the beacons are assumed to be identified correctly. All the distances between the transmitters and receivers are accurately estimated using our ranging algorithm [17]. In the conventional localization methods, these distances are fed to a classical non-linear least squares solver, such as the Gauss-Newton algorithm [18], to obtain the 3D locations of the transmitters. In this paper, the measured distances are exploited by the designed non-convex Riemannian-based optimization algorithms to obtain more accurate location estimates of the three transmitters.

The main contribution of this paper is to provide a novel and highly accurate spatial location estimation method. To that

¹The time of flight is the time required for the signal to travel from the transmitter to the receiver.

Mohammed AlSharif, Mohanad Ahmed, and Tareq Al-Naffouri are with the Division of Computer, Electrical and Mathematical Sciences, and Engineering, King Abdullah University of Science and Technology, Thuwal 23955-6900, Saudi Arabia (e-mail: {mohammed.alsharif,tareq.alnaffouri}@kaust.edu.sa, m.a.m.elhassan@gmail.com).

Ahmed Douik and Babak Hassibi are with the Department of Electrical Engineering, California Institute of Technology, Pasadena, CA 91125 USA (e-mail: {ahmed.douik,hassibi}@caltech.edu).

©2021 IEEE. Personal use of this material is permitted. Permission from IEEE must be obtained for all other uses, in any current or future media, including reprinting/republishing this material for advertising or promotional purposes, creating new collective works, for resale or redistribution to servers or lists, or reuse of any copyrighted component of this work in other works.

end, the transmitters' geometry is integrated into the location estimation process by formulating the problem as a non-convex optimization. Afterward, the set of feasible solutions is shown to admit a Riemannian manifold structure, which allows solving the underlying optimization problem rigorously. To the best of the authors' knowledge, the equilateral triangle manifold has not been introduced nor studied in the literature. Hence, this manuscript characterizes its geometry so as to design Riemannian optimization algorithms for the ultrasound spatial location estimation problem. The efficiency of the proposed method is attested through extensive simulations and comparisons against the-state-of-the-art algorithms in the literature. The numerical results suggest that the inclusion of the fixed equilateral triangle geometry of the transmitters, as non-linear constraints in the optimization problem, significantly improves the quality of the location estimate. In fact, we confirm these results by deriving the Cramér-Rao bound (CRB) and the constrained CRB for our localization setup. Furthermore, the proposed Riemannian-based method offers a clear complexity advantage, evaluated through the computational time, as compared to popular generic non-convex approaches.

The rest of this manuscript is organized as follows. Section II cites and discusses the related work. In Section III, the equilateral triangle geometry of the transmitters is exploited to formulate the ultrasound spatial location estimation problem as a non-convex optimization. A brief overview of Riemannian optimization methods on embedded manifolds is provided in Section IV. Afterward, the equilateral triangle manifold is introduced and investigated in Section V. Given the manifold geometry, Section VI designs efficient algorithms for the location estimation problem. Section VII derives the Cramér-Rao bound (CRB) and the constrained CRB for our localization setup. Finally, before concluding in Section IX, Section VIII presents the simulation results and comparisons with available methods from the literature.

II. RELATED WORK

A significant portion of indoor localization works that are available in the literature utilizes an array of receivers or transmitters to determine the location and orientation of a target. For example, in [19], the authors designed the Active Bat system, which estimates the position and orientation of an array of ultrasound transmitters based on the ToF estimation. The reference suggests performing a nonlinear regression combined with a least-squares solver to obtain the position of the target. The Active Bat system provides an accuracy as high as 3 cm in a 3D space [13]. This accuracy is achieved at the cost of many well-placed beacons. Similarly, the Cricket system is introduced in [20]. The system consists of an array of ultrasound receivers that estimates the time of arrival (ToA) and angle of arrival (AoA) simultaneously. The time and angle of arrival are fed to nonlinear least squares solver to obtain the location and orientation of the target. In contrast to the Active Bat, the Cricket system does not require synchronization between the transmitter and the receiver. However, it achieves an accuracy of 10 cm [21]. In [22], DOLPHIN has been

introduced as a system to localize synchronized nodes in a typical indoor environment. DOLPHIN is similar to the Active Bat and Cricket systems except that it requires only few pre-configured reference nodes. Experimental evaluation of DOLPHIN reports an accuracy of 15 cm in a 2D space with a possible accuracy degradation as we extend of the algorithm to a 3D space. [22].

Combining the ToA and AoA as in [20] results in better performances, which explains their wide adoption in the literature. For example, Saad et al. [23] extend the method to mobile devices in a system that utilizes an array of three receivers. However, instead of relying on a nonlinear least-squares solution, the authors estimate the position of the target through a classical trilateration algorithm. The hybrid method in [23] can achieve a localization accuracy of 7.8 cm [24] at the expense of a higher computational cost to simultaneously estimate the ToF and AoA. Along the same lines, reference [25] considers an array of 8 receivers whose locations are estimated by a Taylor series trilateration method [26]. Finally, the mobile device's position and orientation are obtained based on averaging the AoA and location estimates for the 8 receivers. While the experimental evaluation in [25] reports good location and orientation accuracies, it requires the distances between the receivers to be less than 3.43 mm which is impossible to achieve with conventional ultrasound sensors. The classical trilateration algorithm has been extended in [27] and [28] into a multilateration algorithm for a broadband localization system, with multiple ultrasound transmitters and receivers, as an improvement to the Cricket system. Nevertheless, this enhancement demands costly DSP techniques.

The authors in [29] consider the problem of determining the position of a moving robot in a system comprising an equilateral ultrasound receiver array with a set of transmitters of known locations. The problem is solved by extending the Kalman filter to incorporate a dynamic distance estimation method. The maximum error in the robot position in [29] is 25.7 cm, which is quite large for many location-based applications.

To the best of the authors' knowledge, all previously reported indoor localization systems do not impose the geometry of the receivers array as constraints when solving for the position of the target. Exploiting the fixed geometry of the transmitters or receivers array when formulating the optimization problem is expected to improve the localization estimation accuracy as long as the resulting non-convex problem can be solved efficiently. To that end, the rest of this manuscript formulates the location determination problem as a non-convex program in which the constraints highlight the transmitters' geometry. Afterward, an efficient Riemannian-based optimization algorithm is designed by studying the geometry of the manifold derived from the set of all feasible solutions.

III. LOCATION ESTIMATION USING ULTRASOUND WAVES

A. System Model and Parameters

This paper considers a localization system consisting of three ultrasound transmitters and four receivers, also known as beacons, whose positions are perfectly known. The three

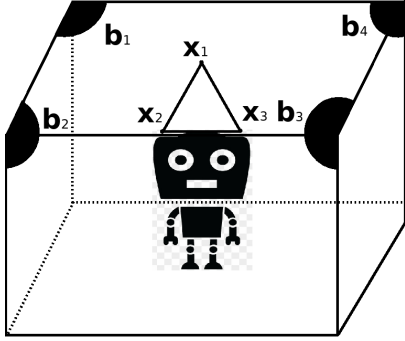


Fig. 1: A localization system consisting of three ultrasound transmitters and four receivers (beacons). The position of the target (robot) with respect to the transmitters is known.

transmitters form an equilateral triangle of side length d as shown in Figure 1. The position of the target of interest is known with respect to the transmitters, e.g., it can be placed in the centroid of the triangle. Therefore, estimating the 3D locations of the three transmitters provides an accurate 3D location and orientation of the target. We would like to mention that swapping the roles of the transmitters and receivers, i.e. a three-receiver array becomes the target and four transmitters become the beacons, won't require any changes in the proposed algorithm.

Let the 3D location of the i -th transmitter be $\mathbf{x}_i \in \mathbb{R}^3$. Likewise, let $\mathbf{b}_j \in \mathbb{R}^3$ denote the position of the j -th beacon. These positions are grouped in a matrix $\mathbf{A} \in \mathbb{R}^{4 \times 3}$ such that the j -th row of the matrix corresponds to the location of the j -th beacon, i.e., $\mathbf{a}_j^T = \mathbf{b}_j^T$ where the notation \mathbf{z}^T refers to the transpose of the vector \mathbf{z} .

Let the received signal from the i^{th} transmitter at the j^{th} receiver be given by [30]

$$\zeta_{ij}(t) = \psi_{ij} s_i(t - \kappa_{ij}) + n_{ij}(t), \quad i = 1, 2, \dots, M, \quad j = 1, 2, \dots, N, \quad (1)$$

where ψ_{ij} is an attenuation factor incurred by propagation, $s_i(t)$ is the passband transmitted signal from the i^{th} transmitter, κ_{ij} is the time of flight (TOF) from the i^{th} transmitter to the j^{th} receiver, M is the number of transmitters, N is the number of receivers, and $n_{ij}(t)$ is an additive Gaussian noise with zero mean and variance σ_{ij}^2 . We obtain the distances between the transmitters and receivers by multiplying the TOF κ_{ij} by the speed of sound. The range r_{ij} , i.e., distance, from the i -th transmitter to the j -th beacon is estimated from the measurements on the received signal using [17] and [31]. It can readily be seen that the distance can be expressed using the vectors \mathbf{x}_i and \mathbf{b}_j as follows

$$r_{ij} = \|\mathbf{x}_i - \mathbf{b}_j\|_2 = \sqrt{(\mathbf{x}_i - \mathbf{b}_j)^T (\mathbf{x}_i - \mathbf{b}_j)}. \quad (2)$$

For ease of notations, the positions, distances, and measurements are collected in vectors as follows

$$\|\mathbf{x}_i\|_2^2 \mathbf{1}_4 = \begin{pmatrix} \|\mathbf{x}_i\|_2^2 \\ \|\mathbf{x}_i\|_2^2 \\ \|\mathbf{x}_i\|_2^2 \\ \|\mathbf{x}_i\|_2^2 \end{pmatrix}, \quad \mathbf{b}^2 = \begin{pmatrix} \|\mathbf{b}_1\|_2^2 \\ \|\mathbf{b}_2\|_2^2 \\ \|\mathbf{b}_3\|_2^2 \\ \|\mathbf{b}_4\|_2^2 \end{pmatrix}, \quad \mathbf{r}_i^2 = \begin{pmatrix} r_{i1}^2 \\ r_{i2}^2 \\ r_{i3}^2 \\ r_{i4}^2 \end{pmatrix},$$

where $\mathbf{1}_4$ is the all ones vector of dimension 4. Define the transformed measurement vector $\mathbf{y}_i = \frac{1}{2}(\mathbf{b}^2 - \mathbf{r}_i^2)$. Using the

expression of r_{ij} 's in (2), it can easily be concluded that

$$\mathbf{A}\mathbf{x}_i - \frac{1}{2}\|\mathbf{x}_i\|_2^2 \mathbf{1}_4 = \mathbf{y}_i \in \mathbb{R}^{4 \times 1}. \quad (3)$$

B. Location Estimation Problem Formulation

This manuscript assumes that all received signals r_{ij} 's, are affected by a normally distributed noise. Therefore, a reasonable objective function is to consider the ℓ_2 loss between the measurement and the model (3). In other words, the paper considers the following objective function

$$\sum_{i=1}^3 \|\mathbf{A}\mathbf{x}_i - \frac{1}{2}\|\mathbf{x}_i\|_2^2 \mathbf{1}_4 - \mathbf{y}_i\|_2^2.$$

The choice of the loss function to be used depends on the assumptions on the system model. While the manuscript focuses on the ℓ_2 loss, the results are more generic and can be applied to any smooth loss function as explained by the end of this section. To incorporate the fixed geometry of the transmitters, the spatial location estimation problem using ultrasound waves can be formulated as

$$\min_{\mathbf{x}_1, \mathbf{x}_2, \mathbf{x}_3 \in \mathbb{R}^3} \sum_{i=1}^3 \|\mathbf{A}\mathbf{x}_i - \frac{1}{2}\|\mathbf{x}_i\|_2^2 \mathbf{1}_4 - \mathbf{y}_i\|_2^2 \quad (4a)$$

$$\text{s.t. } (\mathbf{x}_1 - \mathbf{x}_2)^T (\mathbf{x}_2 - \mathbf{x}_3) = -d^2 \cos\left(\frac{\pi}{3}\right) \quad (4b)$$

$$(\mathbf{x}_1 - \mathbf{x}_3)^T (\mathbf{x}_2 - \mathbf{x}_3) = d^2 \cos\left(\frac{\pi}{3}\right), \quad (4c)$$

wherein constraint (4b) fixes the length and angle of one side of the triangle while equation (4c) constrains the second side. It is worth noting that the constraint on the third side of the triangle is redundant as it can be obtained as a linear combination of constraints (4b) and (4c).

Despite the convexity of the objective function in (4a), the optimization problem is non-convex due to the quadratic nature of the constraints. Indeed, each feasible solution $\mathbf{x}_1, \mathbf{x}_2, \mathbf{x}_3 \in \mathbb{R}^3$ to (4) belongs to a set, named the *equilateral triangle manifold*, which is defined as follows:

$$\mathcal{M} = \left\{ \{\mathbf{x}_i\}_{i=1}^3 \in \mathbb{R}^3 \mid \begin{aligned} &(\mathbf{x}_1 - \mathbf{x}_2)^T (\mathbf{x}_2 - \mathbf{x}_3) = -d^2 \cos\left(\frac{\pi}{3}\right) \\ &(\mathbf{x}_1 - \mathbf{x}_3)^T (\mathbf{x}_2 - \mathbf{x}_3) = d^2 \cos\left(\frac{\pi}{3}\right) \end{aligned} \right\}.$$

It is straightforward to show that the set \mathcal{M} is non-convex. However, as shown in Section V, it forms a closed and bounded, i.e., a compact, matrix manifold embedded in the Euclidean space $\mathbb{R}^{3 \times 3}$. Therefore, the study of the geometry of this newly introduced manifold allows to take advantage of Riemannian optimization methods to efficiently solve the location estimation problem. Furthermore, instead of directly solving the optimization problem (4), this manuscript suggest solving its generalization. In particular, let $\{\mathbf{x}_i\}_{i=1}^3$ be 3-dimensional vectors in \mathbb{R}^3 and consider a smooth function $f : (\mathbb{R}^3)^3 \rightarrow \mathbb{R}$, that may or may not be convex, the rest of this manuscript solves the optimization problem

$$\min_{\mathbf{x}_1, \mathbf{x}_2, \mathbf{x}_3 \in \mathbb{R}^3} f(\mathbf{x}_1, \mathbf{x}_2, \mathbf{x}_3) \quad (5a)$$

$$\text{s.t. } (\mathbf{x}_1, \mathbf{x}_2, \mathbf{x}_3) \in \mathcal{M}. \quad (5b)$$

IV. OPTIMIZATION ON RIEMANNIAN MANIFOLDS

This manuscript uses Riemannian manifold optimization to solve the location estimation problem described in the previous section. In this paper, we consider submanifolds of Euclidean spaces equipped with the corresponding Euclidean metric. Since this section succinctly introduces all the required ingredients by presenting an overview of Riemannian optimization methods over matrix manifolds [32], no prior knowledge of differential geometry or Riemannian manifold is required from the reader. More specifically, while Subsection IV-A recalls all necessary manifold terminology, definitions, and notations, Subsection IV-B illustrates the design of a Riemannian optimization algorithm and recalls relevant convergence results. For more details on Riemannian optimization we refer the reader to [32], [33], and [34].

A. Manifold Terminology, Definitions, and Notations

A matrix manifold \mathcal{M} embedded in the Euclidean space of matrices $\mathcal{E} = \mathbb{R}^{n \times m}$ is a subset of \mathcal{E} that is in bijection with an open space $\mathcal{E}^* \subseteq \mathcal{E}$. At each point $\mathbf{X} \in \mathcal{M}$, the manifold can be locally approximated by a ρ -dimensional linear space known as the *tangent space* and denoted by $\mathcal{T}_{\mathbf{X}}\mathcal{M}$. Tangent spaces play a primordial role in designing optimization algorithms in the same fashion as derivatives are crucial to approximate functions. Indeed, the tangent space $\mathcal{T}_{\mathbf{X}}\mathcal{M}$ at $\mathbf{X} \in \mathcal{M}$ can be seen as a local linearization of the manifold \mathcal{M} around \mathbf{X} . Furthermore, the dimension ρ of $\mathcal{T}_{\mathbf{X}}\mathcal{M}$ is said to be the dimension of the manifold \mathcal{M} as it represents its degrees of freedom.

In order to perform optimization on a manifold \mathcal{M} , one needs the notion of length that applies to tangent vectors. This is accomplished by endowing each tangent space $\mathcal{T}_{\mathbf{X}}\mathcal{M}$ by an inner product $\langle \cdot, \cdot \rangle_{\mathbf{X}}$ that is smoothly varying for $\mathbf{X} \in \mathcal{M}$. This smoothly varying inner product is known as the Riemannian metric, and the manifold \mathcal{M} is called a Riemannian manifold [32]. While there exist multiple Riemannian metrics for a manifold \mathcal{M} , a canonical choice for embedded matrix manifolds is the canonical inner product of the matrix space. A particular property of induced Riemannian metrics from the Euclidean space of matrices is that they do not depend on the origin of the tangent space, i.e., $\langle \cdot, \cdot \rangle_{\mathbf{X}} = \langle \cdot, \cdot \rangle$ for any $\mathbf{X} \in \mathcal{M}$. The rest of this manuscript assumes that the canonical Riemannian metric is utilized as it allows to simplify the expressions of the geometry of the manifold, e.g., gradient, covariant derivative, and Hessian.

Let $f : \mathcal{M} \rightarrow \mathbb{R}$ be a smooth function from the matrix manifold \mathcal{M} to \mathbb{R} and let $\mathbf{X} \in \mathcal{M}$ be a point on the manifold. Consider a tangent vector $\xi_{\mathbf{X}} \in \mathcal{T}_{\mathbf{X}}\mathcal{M}$, the derivative of $f(\mathbf{X})$ in the direction $\xi_{\mathbf{X}}$, denoted by $D(f(\mathbf{X}))[\xi_{\mathbf{X}}]$, is defined as

$$D(f(\mathbf{X}))[\xi_{\mathbf{X}}] = \lim_{h \rightarrow 0} \frac{f(\mathbf{X} + h\xi_{\mathbf{X}}) - f(\mathbf{X})}{h}.$$

One can note that the above definition of directional derivatives is closely related to the one for Euclidean spaces with the exception that only tangent vectors $\xi_{\mathbf{X}} \in \mathcal{T}_{\mathbf{X}}\mathcal{M}$ are permitted as perturbations. Indeed, while the expression $f(\mathbf{X} + \mathbf{Y})$ is well defined for a Euclidean space \mathcal{E} thanks to the fact that $\mathbf{X} + \mathbf{Y} \in \mathcal{E}$ for all vectors $\mathbf{X}, \mathbf{Y} \in \mathcal{E}$, for a Riemannian

Algorithm 1 Template of Unconstrained Optimization

- 1: Initialize $\mathbf{X} \in \mathcal{E}$.
 - 2: **while** $\|\nabla_{\mathbf{X}}f\| \neq 0$ **do**
 - 3: Find a descent direction $\xi \in \mathcal{E}$ using $\nabla_{\mathbf{X}}f$ and/or $\nabla_{\mathbf{X}}^2f$
 - 4: Compute a step size α .
 - 5: update $\mathbf{X} = \mathbf{X} + \alpha\xi$.
 - 6: **end while**
-

manifold \mathcal{M} , the expression $f(\mathbf{X} + h\xi_{\mathbf{X}})$ is only valid for a tangent vector $\xi_{\mathbf{X}} \in \mathcal{T}_{\mathbf{X}}\mathcal{M}$ and a small perturbation $h \ll 1$. In fact, as stated earlier, the tangent space $\mathcal{T}_{\mathbf{X}}\mathcal{M}$ is only a linear approximation of the manifold locally around \mathbf{X} . The indefinite directional derivative of f at \mathbf{X} is defined as the operator $D(f(\mathbf{X})) : \mathcal{T}_{\mathbf{X}}\mathcal{M} \rightarrow \mathbb{R}$ which associates to each $\xi_{\mathbf{X}}$ the directional derivative $D(f(\mathbf{X}))[\xi_{\mathbf{X}}]$.

B. Optimization Over Matrix Manifolds

Riemannian optimization is an extension of unconstrained iterative optimization methods from Euclidean spaces to Riemannian manifolds. In other words, Riemannian optimization methods can be seen as unconstrained optimization over a constrained set, i.e., a manifold. Recall that unconstrained Euclidean optimization starts with an initial guess $\mathbf{X} \in \mathcal{E}$ and at each iteration finds a descent direction ξ and a step size α to update the point through $\mathbf{X} = \mathbf{X} + \alpha\xi$. The aforementioned steps of unconstrained Euclidean Optimization are summarized in Algorithm 1.

As stated earlier, Riemannian optimization extends Algorithm 1 to Riemannian manifolds. While unconstrained optimization initialize with any $\mathbf{X} \in \mathcal{E}$, Riemannian optimization require a feasible point $\mathbf{X} \in \mathcal{M}$. Afterward, the curvature of the manifold is approximated locally around \mathbf{X} by a linear ρ -dimensional space through the computation of the tangent space $\mathcal{T}_{\mathbf{X}}\mathcal{M}$. Since the tangent space is linear, one can find a descent direction in that tangent space using the same technique as for unconstrained optimization. However, this requires the introduction of the Riemannian gradient $\overline{\nabla}_{\mathbf{X}}f$ and Hessian $\overline{\nabla}_{\mathbf{X}}^2f$ as the Euclidean gradient $\nabla_{\mathbf{X}}f$ and Hessian $\nabla_{\mathbf{X}}^2f$ are defined on the original high-dimensional space \mathcal{E} and not exclusively on $\mathcal{T}_{\mathbf{X}}\mathcal{M}$.

Thanks to the use of the canonical Riemannian metric induced from the embedding space, the Riemannian gradient $\overline{\nabla}_{\mathbf{X}}f$ can be obtained by simply projecting the Euclidean gradient $\nabla_{\mathbf{X}}f$ onto the tangent space $\mathcal{T}_{\mathbf{X}}\mathcal{M}$, i.e., $\overline{\nabla}_{\mathbf{X}}f = \Pi_{\mathbf{X}}(\nabla_{\mathbf{X}}f)$. Such an orthogonal projection $\Pi_{\mathbf{X}}$, i.e. orthogonal according to the Riemannian metric, onto the tangent space $\mathcal{T}_{\mathbf{X}}\mathcal{M}$ is well defined for any $\mathbf{X} \in \mathcal{M}$ due to the linear structure of the tangent space. Similarly, the definition of Riemannian Hessian $\overline{\nabla}_{\mathbf{X}}^2f$ follow that of the Euclidean Hessian which is obtained as the directional derivative of the gradient, i.e., $\nabla_{\mathbf{X}}^2f[\xi_{\mathbf{X}}] = D(\nabla_{\mathbf{X}}f)[\xi_{\mathbf{X}}]$. However, as the directional derivative of the Riemannian gradient may not be contained in the tangent space, the Riemannian Hessian requires projecting the directional derivative of the Riemannian gradient onto the tangent space, i.e.,

$$\overline{\nabla}_{\mathbf{X}}^2f[\xi_{\mathbf{X}}] = \Pi_{\mathbf{X}}(D(\overline{\nabla}_{\mathbf{X}}f)[\xi_{\mathbf{X}}]) \quad (6)$$

Algorithm 2 Template of Riemannian Optimization

- 1: Initialize $\mathbf{X} \in \mathcal{M}$.
 - 2: **while** $\|\bar{\nabla}_{\mathbf{X}} f\|_{\mathbf{X}} \neq 0$ **do**
 - 3: Find a descent direction $\xi_{\mathbf{X}} \in \mathcal{T}_{\mathbf{X}}\mathcal{M}$ using $\bar{\nabla}_{\mathbf{X}} f$ and/or $\frac{\bar{\nabla}_{\mathbf{X}}^2 f}{\|\bar{\nabla}_{\mathbf{X}} f\|_{\mathbf{X}}}$
 - 4: Compute the step size α using backtracking.
 - 5: Retract $\mathbf{X} = \mathbf{R}_{\mathbf{X}}(\alpha\xi_{\mathbf{X}})$.
 - 6: **end while**
-

Finally, after we obtain a descent direction $\xi_{\mathbf{X}}$, and a step size α depending on the employed algorithm, Euclidean algorithms update the current position through the linear equation $\mathbf{X} = \mathbf{X} + \alpha\xi_{\mathbf{X}}$. While such an update is valid for linear spaces, it does not apply to Riemannian manifolds as it might result in a point outside the manifold. Therefore, one needs to “project” such an update on the manifold while conserving its descent property. This is naturally accomplished by moving along geodesics, i.e., straight lines, on the manifold. However, finding the expression of geodesics can be difficult [35] which motivates the use of their first order approximation known as *retractions*. In particular, a retraction $\mathbf{R}_{\mathbf{X}} : \mathcal{T}_{\mathbf{X}}\mathcal{M} \rightarrow \mathcal{M}$ is a mapping from tangent vectors to the manifold such as $\mathbf{R}_{\mathbf{X}}(\mathbf{0}_{\mathbf{X}}) = \mathbf{X}$ and $\left. \frac{d \mathbf{R}_{\mathbf{X}}(h\xi_{\mathbf{X}})}{dh} \right|_{h=0} = \xi_{\mathbf{X}}$. Therefore, deriving a computationally efficient retraction is a critical and delicate step in designing Riemannian optimization algorithms.

The steps of Riemannian optimization methods are summarized in the template shown in Algorithm 2. Unlike the unconstrained optimization in Algorithm 1, Algorithm 2 requires the point \mathbf{X} to be on the manifold, and the descent direction to be on the tangent space. In the rest of this manuscript, an instance of Algorithm 2 in which the descent direction only requires the gradient information is referred to as a first order Riemannian optimization algorithm while the use of the Riemannian Hessian elevates the algorithm to second order.

For example, choosing $\xi_{\mathbf{X}} = -\frac{\bar{\nabla}_{\mathbf{X}} f}{\|\bar{\nabla}_{\mathbf{X}} f\|_{\mathbf{X}}}$ yields the celebrated steepest descent algorithm on Riemannian manifolds [32]. Likewise, Newton’s method on Riemannian manifolds, a second order algorithm, is obtained by finding the tangent vector $\xi_{\mathbf{X}} \in \mathcal{T}_{\mathbf{X}}\mathcal{M}$ that satisfies the following Newton’s equation $\bar{\nabla}_{\mathbf{X}}^2 f[\xi_{\mathbf{X}}] = -\bar{\nabla}_{\mathbf{X}} f$.

For compact manifolds and smooth objective functions, first and second order Riemannian methods are guaranteed to converge to a critical point of the optimization problem [35], i.e., a zero of the gradient of the Lagrangian function associated with the optimization problem [36].

V. THE EQUILATERAL TRIANGLE MANIFOLD

This section investigates and characterizes the geometry of the equilateral triangle manifold so as to employ, in Section VI, optimization algorithms for the location estimation problem of interest in this paper. These optimization algorithms are guaranteed to converge to a critical point, thanks to the compactness of the equilateral triangle manifold and the smoothness of the objective function (5). The first part of the section shows that the set is indeed a manifold and computes its tangent space

and orthogonal projection. The second and third parts of the section compute the expression of the Riemannian gradient and Hessian and derive a computationally efficient retraction of the equilateral triangle manifold.

For conciseness and ease of notations, the variable $\mathbf{X} \in \mathbb{R}^{3 \times 3}$ is used in the rest of this manuscript as a shorthand notation for the three vectors $\mathbf{X} = [\mathbf{x}_1, \mathbf{x}_2, \mathbf{x}_3]$. Similarly, the tangent vector at $\mathbf{X} = [\mathbf{x}_1, \mathbf{x}_2, \mathbf{x}_3]$ is denoted by $\xi_{\mathbf{X}} = [\xi_{\mathbf{x}_1}, \xi_{\mathbf{x}_2}, \xi_{\mathbf{x}_3}] \in \mathbb{R}^{3 \times 3}$.

A. Manifold Geometry and Operators

Recall that the equilateral triangle manifold is defined by
$$\mathcal{M} = \left\{ \mathbf{X} \in \mathbb{R}^{3 \times 3} \mid \begin{aligned} (\mathbf{x}_1 - \mathbf{x}_2)^T (\mathbf{x}_2 - \mathbf{x}_3) &= -d^2 \cos\left(\frac{\pi}{3}\right) \\ (\mathbf{x}_1 - \mathbf{x}_3)^T (\mathbf{x}_2 - \mathbf{x}_3) &= d^2 \cos\left(\frac{\pi}{3}\right) \end{aligned} \right\}. \quad (7)$$

To show that the set defined in (7) is a well-defined manifold and to compute its tangent space, this section uses the implicit function theorem [35] which can be formulated as follows

Theorem 1. *Let \mathcal{E} be a Euclidean space and let $g : \mathcal{E} \rightarrow \mathcal{E}'$ be a smooth and constant-rank function from \mathcal{E} to a linear space \mathcal{E}' . Under the above conditions, any level-set \mathcal{M} of g admits a manifold structure. Furthermore, the tangent space at $\mathbf{X} \in \mathcal{M}$ is given by*

$$\mathcal{T}_{\mathbf{X}}\mathcal{M} = \text{Ker}(D(g(\mathbf{X}))).$$

First of all, we show that the set \mathcal{M} defined in (7) admits a manifold structure. Therefore, we define a function $g : \mathbb{R}^{3 \times 3} \rightarrow \mathbb{R}^2$ as

$$g(\mathbf{X}) = \begin{pmatrix} (\mathbf{x}_1 - \mathbf{x}_2)^T (\mathbf{x}_2 - \mathbf{x}_3) + d^2 \cos\left(\frac{\pi}{3}\right) \\ (\mathbf{x}_1 - \mathbf{x}_3)^T (\mathbf{x}_2 - \mathbf{x}_3) - d^2 \cos\left(\frac{\pi}{3}\right) \end{pmatrix}. \quad (8)$$

The above defined function only involves linear combinations and inner products of the vectors which makes it smooth as required by the implicit function theorem. In addition, the set of 2-dimensional vectors \mathbb{R}^2 is a linear space as mandated by Theorem 1. From the definition of the function g and the set \mathcal{M} in (7), it is clear that \mathcal{M} is a level-set of g as it can be interpreted as the image of $\mathbf{0} \in \mathbb{R}^2$.

Lastly, according to Theorem 1, to prove that \mathcal{M} is a well-defined manifold we need to show that g is a constant-rank function, which can be accomplished by demonstrating that $\mathbf{0}$ is a regular value of g , i.e., the rank of each $\mathbf{X} \in g^{-1}(\mathbf{0}) = \mathcal{M}$ is equal to $\text{Dim}(\mathbb{R}^2) = 2$ or equivalently that the indefinite directional derivative of g at any $\mathbf{X} \in \mathcal{M}$ is a surjective map. Let $\mathbf{X} \in \mathcal{M}$ and consider an arbitrary direction $\xi_{\mathbf{X}} \in \mathbb{R}^{3 \times 3}$, the directional derivative of g at \mathbf{X} in the direction $\xi_{\mathbf{X}}$ is

$$D(g(\mathbf{X}))[\xi_{\mathbf{X}}] = \begin{pmatrix} ((\xi_{\mathbf{x}_1} - \xi_{\mathbf{x}_2})^T (\mathbf{x}_2 - \mathbf{x}_3) + (\mathbf{x}_1 - \mathbf{x}_2)^T (\xi_{\mathbf{x}_2} - \xi_{\mathbf{x}_3})) \\ ((\xi_{\mathbf{x}_1} - \xi_{\mathbf{x}_3})^T (\mathbf{x}_2 - \mathbf{x}_3) + (\mathbf{x}_1 - \mathbf{x}_3)^T (\xi_{\mathbf{x}_2} - \xi_{\mathbf{x}_3})) \end{pmatrix}. \quad (9)$$

Let $\begin{pmatrix} \alpha \\ \beta \end{pmatrix}$ be an arbitrary vector in \mathbb{R}^2 . Finding $\xi_{\mathbf{X}} \in \mathbb{R}^{3 \times 3}$

such that $D(g(\mathbf{X}))[\xi_{\mathbf{X}}] = \begin{pmatrix} \alpha \\ \beta \end{pmatrix}$ amounts to solving the following linear system of equations

$$\begin{pmatrix} \mathbf{x}_2 - \mathbf{x}_3 & \mathbf{x}_2 - \mathbf{x}_3 \\ \mathbf{x}_1 + \mathbf{x}_3 - 2\mathbf{x}_2 & \mathbf{x}_1 - \mathbf{x}_3 \\ \mathbf{x}_2 - \mathbf{x}_1 & 2\mathbf{x}_3 - \mathbf{x}_1 - \mathbf{x}_2 \end{pmatrix}^T \begin{pmatrix} \xi_{\mathbf{x}_1} \\ \xi_{\mathbf{x}_2} \\ \xi_{\mathbf{x}_3} \end{pmatrix} = \begin{pmatrix} \alpha \\ \beta \end{pmatrix}.$$

The above linear system has a fat matrix of dimension 2×3 and a full rank 2. Indeed, assuming that the rank is equal to 1 gives the equality $\mathbf{x}_2 = \mathbf{x}_3$ which is impossible for any $\mathbf{X} \in \mathcal{M}$. Therefore, it holds true that the map $D(g(\mathbf{X}))$ is surjective which concludes that the function g is a constant rank function. Therefore, according to the results of Theorem 1, we conclude that the equilateral triangle set \mathcal{M} defined in (7) is a well-defined manifold of dimension 7 embedded in the Euclidean space $\mathbb{R}^{3 \times 3}$.

After we have shown that the set \mathcal{M} admits a manifold structure, we derive its tangent space. According to Theorem 1, the tangent space is given by all directions $\xi_{\mathbf{X}} \in \mathbb{R}^{3 \times 3}$ that nullify $D(g(\mathbf{X}))[\xi_{\mathbf{X}}]$, which according to the expression given in (9) can be written as

$$\begin{aligned} \mathcal{T}_{\mathbf{X}}\mathcal{M} = \left\{ \xi_{\mathbf{X}} \in \mathbb{R}^{3 \times 3} \mid \right. \\ \left. \begin{aligned} (\xi_{\mathbf{x}_1} - \xi_{\mathbf{x}_2})^T(\mathbf{x}_2 - \mathbf{x}_3) + (\mathbf{x}_1 - \mathbf{x}_2)^T(\xi_{\mathbf{x}_2} - \xi_{\mathbf{x}_3}) = 0 \\ (\xi_{\mathbf{x}_1} - \xi_{\mathbf{x}_3})^T(\mathbf{x}_2 - \mathbf{x}_3) + (\mathbf{x}_1 - \mathbf{x}_3)^T(\xi_{\mathbf{x}_2} - \xi_{\mathbf{x}_3}) = 0 \end{aligned} \right\}. \end{aligned} \quad (10)$$

As stated earlier, this manuscript considers the induced Riemannian metric from canonical inner product $\langle \mathbf{X}, \mathbf{Y} \rangle = \text{Tr}(\mathbf{X}^T \mathbf{Y})$ in $\mathbb{R}^{3 \times 3}$. In other words, the induced Riemannian metric on the tangent space $\mathcal{T}_{\mathbf{X}}\mathcal{M}$ is obtained from the natural embedding of \mathcal{M} in $\mathbb{R}^{3 \times 3}$, i.e.,

$$\langle \xi_{\mathbf{X}}, \eta_{\mathbf{X}} \rangle_{\mathbf{X}} = \text{Tr}(\xi_{\mathbf{X}}^T \eta_{\mathbf{X}}) = \xi_{\mathbf{x}_1}^T \eta_{\mathbf{x}_1} + \xi_{\mathbf{x}_2}^T \eta_{\mathbf{x}_2} + \xi_{\mathbf{x}_3}^T \eta_{\mathbf{x}_3}.$$

B. Riemannian Gradient and Hessian

In this part, we derive the expression of the Riemannian gradient and Hessian. According to Section IV, the Riemannian gradient $\bar{\nabla}_{\mathbf{X}} f$ can be expressed as the orthogonal projection, denoted as $\Pi_{\mathbf{X}} : \mathbb{R}^{3 \times 3} \rightarrow \mathcal{T}_{\mathbf{X}}\mathcal{M}$, of the Euclidean gradient from the embedding space $\mathbb{R}^{3 \times 3}$ to the tangent space $\mathcal{T}_{\mathbf{X}}\mathcal{M}$.

In order to derive the orthogonal projection, we start by defining the orthogonal complement $\mathcal{T}_{\mathbf{X}}^{\perp}\mathcal{M}$ to the tangent space $\mathcal{T}_{\mathbf{X}}\mathcal{M}$ at $\mathbf{X} \in \mathcal{M}$ as

$$\mathcal{T}_{\mathbf{X}}^{\perp}\mathcal{M} = \left\{ \eta_{\mathbf{X}} \in \mathbb{R}^{3 \times 3} \mid \eta_{\mathbf{X}} = \mathbf{X}\mathbf{U}_{\alpha}^{\beta} \right\},$$

for some reals α and β and the matrix $\mathbf{U}_{\alpha}^{\beta}$ being constructed as

$$\mathbf{U}_{\alpha}^{\beta} = \begin{pmatrix} 0 & \alpha + \beta & -\alpha - \beta \\ \alpha + \beta & -2\alpha & \alpha - \beta \\ -\alpha - \beta & \alpha - \beta & 2\beta \end{pmatrix}.$$

Indeed, consider a tangent vector $\xi_{\mathbf{X}} \in \mathcal{T}_{\mathbf{X}}\mathcal{M}$ and a normal vector $\eta_{\mathbf{X}} \in \mathcal{T}_{\mathbf{X}}^{\perp}\mathcal{M}$, then their inner product after expansion is given by

$$\begin{aligned} \langle \xi_{\mathbf{X}}, \eta_{\mathbf{X}} \rangle_{\mathbf{X}} &= \xi_{\mathbf{x}_1}^T \eta_{\mathbf{x}_1} + \xi_{\mathbf{x}_2}^T \eta_{\mathbf{x}_2} + \xi_{\mathbf{x}_3}^T \eta_{\mathbf{x}_3} \\ &= \alpha [(\xi_{\mathbf{x}_1} - \xi_{\mathbf{x}_2})^T(\mathbf{x}_2 - \mathbf{x}_3) + (\mathbf{x}_1 - \mathbf{x}_2)^T(\xi_{\mathbf{x}_2} - \xi_{\mathbf{x}_3})] \\ &\quad + \beta [(\xi_{\mathbf{x}_1} - \xi_{\mathbf{x}_3})^T(\mathbf{x}_2 - \mathbf{x}_3) + (\mathbf{x}_1 - \mathbf{x}_3)^T(\xi_{\mathbf{x}_2} - \xi_{\mathbf{x}_3})] \\ &= 0. \end{aligned}$$

Combining the above equality with the fact that $\mathcal{T}_{\mathbf{X}}^{\perp}\mathcal{M}$ is a Euclidean space of dimension 2 allows us to conclude that $\mathcal{T}_{\mathbf{X}}^{\perp}\mathcal{M}$ represents the complement of the tangent space.

The next stage is to derive the orthogonal projection from the embedding space to the tangent space, by utilizing the complement to the tangent space. Let $\mathbf{Z} \in \mathbb{R}^{3 \times 3}$ be a vector in the ambient space and $\mathbf{X} \in \mathcal{M}$ be a point on the manifold. The vector \mathbf{Z} can be decomposed into a tangent part $\Pi_{\mathbf{X}}(\mathbf{Z}) =$

$\mathbf{Z}_{\mathbf{X}} \in \mathcal{T}_{\mathbf{X}}\mathcal{M}$ and an orthogonal part $\Pi_{\mathbf{X}}^{\perp}(\mathbf{Z}) = \mathbf{Z}_{\mathbf{X}}^{\perp} \in \mathcal{T}_{\mathbf{X}}^{\perp}\mathcal{M}$. From the previous analysis of the orthogonal complement of the tangent space, the orthogonal vector $\mathbf{Z}_{\mathbf{X}}^{\perp}$ is parametrized by two reals α and β such that $\mathbf{Z}_{\mathbf{X}}^{\perp} = \mathbf{X}\mathbf{U}_{\alpha}^{\beta}$. Lastly, using the fact that the tangent vector $\mathbf{Z}_{\mathbf{X}}$ satisfies the equations in (10), we conclude that the reals α and β are the solution to

$$\begin{pmatrix} \|\mathbf{X}\mathbf{U}_1^0\|_{\mathbf{X}}^2 & \langle \mathbf{X}\mathbf{U}_0^1, \mathbf{X}\mathbf{U}_1^0 \rangle_{\mathbf{X}} \\ \langle \mathbf{X}\mathbf{U}_1^0, \mathbf{X}\mathbf{U}_0^1 \rangle_{\mathbf{X}} & \|\mathbf{X}\mathbf{U}_0^1\|_{\mathbf{X}}^2 \end{pmatrix} \begin{pmatrix} \alpha \\ \beta \end{pmatrix} = \begin{pmatrix} \langle \mathbf{Z}, \mathbf{X}\mathbf{U}_1^0 \rangle_{\mathbf{X}} \\ \langle \mathbf{Z}, \mathbf{X}\mathbf{U}_0^1 \rangle_{\mathbf{X}} \end{pmatrix}. \quad (11)$$

The above linear system of equations admits a unique solution. Indeed, matrix \mathbf{S} defined by

$$\mathbf{S} = \begin{pmatrix} \|\mathbf{X}\mathbf{U}_1^0\|_{\mathbf{X}}^2 & \langle \mathbf{X}\mathbf{U}_0^1, \mathbf{X}\mathbf{U}_1^0 \rangle_{\mathbf{X}} \\ \langle \mathbf{X}\mathbf{U}_1^0, \mathbf{X}\mathbf{U}_0^1 \rangle_{\mathbf{X}} & \|\mathbf{X}\mathbf{U}_0^1\|_{\mathbf{X}}^2 \end{pmatrix} \quad (12)$$

is a positive definite matrix with $\lambda_1^2 + \lambda_2^2 = \|\mathbf{S}\|_F^2 < \text{Tr}^2(\mathbf{S}) = (\lambda_1 + \lambda_2)^2$, i.e., $\lambda_1 \lambda_2 \neq 0$, where λ_1 and λ_2 are the eigenvalues of the matrix \mathbf{S} . Therefore, the orthogonal projection onto the tangent space is given by

$$\Pi_{\mathbf{X}}(\mathbf{Z}) = \mathbf{Z} - \mathbf{X}\mathbf{U}_{\alpha}^{\beta} \quad (13)$$

with α and β defined as the solution to the linear system (11).

Finally, applying the orthogonal projection $\Pi_{\mathbf{X}}$ to the Euclidean gradient $\nabla_{\mathbf{X}} f$ results in the expression of the Riemannian gradient $\bar{\nabla}_{\mathbf{X}} f$ as follows:

$$\bar{\nabla}_{\mathbf{X}} f = \nabla_{\mathbf{X}} f - \mathbf{X}\mathbf{U}_{\alpha}^{\beta} \quad (14)$$

with the reals α and β being the solution to the linear system

$$\mathbf{S} \begin{pmatrix} \alpha \\ \beta \end{pmatrix} = \begin{pmatrix} \langle \nabla_{\mathbf{X}} f, \mathbf{X}\mathbf{U}_1^0 \rangle_{\mathbf{X}} \\ \langle \nabla_{\mathbf{X}} f, \mathbf{X}\mathbf{U}_0^1 \rangle_{\mathbf{X}} \end{pmatrix}. \quad (15)$$

Given the expression of the Riemannian gradient in (14), the Riemannian Hessian can be computed as the orthogonal projection of the directional derivative of the Riemannian gradient as illustrated in (6). Let $\mathbf{X} \in \mathcal{M}$ be a vector on the manifold, $\xi_{\mathbf{X}} \in \mathcal{T}_{\mathbf{X}}\mathcal{M}$ a tangent vector, and $f : \mathcal{M} \rightarrow \mathbb{R}$ a smooth function. The rest of this manuscript uses the shorthand notation $\dot{f}(\mathbf{X})$ to denote the directional derivative $D(f(\mathbf{X}))[\xi_{\mathbf{X}}]$. Using the previously defined dot notation, the expression of the Riemannian Hessian is provided in the following corollary.

Corollary 1. *The Riemannian Hessian for the equilateral triangle manifold has the expression*

$$\bar{\nabla}_{\mathbf{X}}^2 f[\xi_{\mathbf{X}}] = \Pi_{\mathbf{X}}(\nabla_{\mathbf{X}}^2 f[\xi_{\mathbf{X}}] - \xi_{\mathbf{X}}\mathbf{U}_{\alpha}^{\beta} - \mathbf{X}\dot{\mathbf{U}}_{\alpha}^{\beta}), \quad (16)$$

wherein the expression of the orthogonal projection $\Pi_{\mathbf{X}}$ is given in (13) and α and β are the solution to (15), wherein \mathbf{S} is given in (12), and their directional derivatives $\dot{\alpha}$ and $\dot{\beta}$ are the solution to the system

$$\mathbf{S} \begin{pmatrix} \dot{\alpha} \\ \dot{\beta} \end{pmatrix} = \begin{pmatrix} \langle \nabla_{\mathbf{X}}^2 f[\xi_{\mathbf{X}}], \mathbf{X}\mathbf{U}_1^0 \rangle_{\mathbf{X}} + \langle \nabla_{\mathbf{X}} f, \xi_{\mathbf{X}}\mathbf{U}_1^0 \rangle_{\mathbf{X}} \\ \langle \nabla_{\mathbf{X}}^2 f[\xi_{\mathbf{X}}], \mathbf{X}\mathbf{U}_0^1 \rangle_{\mathbf{X}} + \langle \nabla_{\mathbf{X}} f, \xi_{\mathbf{X}}\mathbf{U}_0^1 \rangle_{\mathbf{X}} \end{pmatrix} - \dot{\mathbf{S}} \begin{pmatrix} \alpha \\ \beta \end{pmatrix},$$

and the directional derivative of \mathbf{S} in the direction $\xi_{\mathbf{X}}$ is

$$\dot{\mathbf{S}} = \left(\begin{array}{c|c} 2\langle \xi_{\mathbf{X}}\mathbf{U}_1^0, \mathbf{X}\mathbf{U}_1^0 \rangle_{\mathbf{X}} & \langle \xi_{\mathbf{X}}\mathbf{U}_0^1, \mathbf{X}\mathbf{U}_1^0 \rangle_{\mathbf{X}} \\ \langle \xi_{\mathbf{X}}\mathbf{U}_1^0, \mathbf{X}\mathbf{U}_0^1 \rangle_{\mathbf{X}} & + \langle \mathbf{X}\mathbf{U}_0^1, \xi_{\mathbf{X}}\mathbf{U}_1^0 \rangle_{\mathbf{X}} \\ \hline \langle \xi_{\mathbf{X}}\mathbf{U}_1^0, \mathbf{X}\mathbf{U}_0^1 \rangle_{\mathbf{X}} & 2\langle \xi_{\mathbf{X}}\mathbf{U}_0^1, \mathbf{X}\mathbf{U}_0^1 \rangle_{\mathbf{X}} \\ + \langle \mathbf{X}\mathbf{U}_1^0, \xi_{\mathbf{X}}\mathbf{U}_0^1 \rangle_{\mathbf{X}} & \end{array} \right).$$

Proof. The proof of this corollary is omitted herein as it follows from a direct computation of the orthogonal projection of the directional derivative of the Riemannian gradient. ■

C. Retraction on the Equilateral Triangle Manifold

Designing a computationally efficient retraction is a crucial step in deriving Riemannian optimization algorithms. While it is relatively easy to design functions that are local retractions around $\mathbf{0}_{\mathbf{X}}$, e.g., $R_{\mathbf{X}}(\xi_{\mathbf{X}}) = \mathbf{X} + \xi_{\mathbf{X}}$, these retractions often result in Riemannian algorithms with poor performance. Indeed, the resulting iterative optimization algorithm would generate smaller and smaller optimization steps ultimately converging before reaching a critical point of the problem. Luckily, for manifolds defined with only equality constraints such as the equilateral triangle manifold of interest in this paper, the following theorem allows to design retractions that are valid for all tangent vectors [32]

Theorem 2. *Consider an embedded manifold \mathcal{M} in the Euclidean space \mathcal{E} and let \mathcal{N} be an abstract manifold such that $\dim(\mathcal{M}) + \dim(\mathcal{N}) = \dim(\mathcal{E})$. Let \mathcal{E}^* be an open subset of \mathcal{E} and assume that there is a diffeomorphism function $\phi : \mathcal{M} \times \mathcal{N} \rightarrow \mathcal{E}^*$, i.e., ϕ is smooth and bijective function with ϕ^{-1} also being smooth. Furthermore, assume there exists an element $\mathbf{I} \in \mathcal{N}$ satisfying $\phi(\mathbf{X}, \mathbf{I}) = \mathbf{X}$, $\forall \mathbf{X} \in \mathcal{M}$. Under the above assumption, the mapping $R_{\mathbf{X}}(\xi_{\mathbf{X}}) = \pi_1(\phi^{-1}(\mathbf{X} + \xi_{\mathbf{X}}))$, where $\pi_1(\mathbf{X}, \mathbf{Y}) = \mathbf{X}$, defines a retraction on the manifold \mathcal{M} for all tangent vectors $\xi_{\mathbf{X}} \in \mathcal{T}_{\mathbf{X}}\mathcal{M}$ [32].*

The rest of this section exploits the result of Theorem 2 to design a computationally efficient retraction. To that end, define \mathcal{E}^* as a subset of $\mathbb{R}^{3 \times 3}$ such that $\mathbf{Z} \in \mathcal{E}^*$ implies that $\mathbf{z}_2 \neq \pm \mathbf{z}_3$. It can easily be seen that \mathcal{E}^* is an open subset of $\mathbb{R}^{3 \times 3}$. Furthermore, let $\mathcal{N} = \mathbb{R}_*^2$ be the set of 2-dimensional vectors $\begin{pmatrix} \alpha \\ \beta \end{pmatrix}$ such that $\alpha \neq 0$ and $\beta \neq 0$. Since $\dim(\mathcal{N}) = 2$, the property $\dim(\mathcal{M}) + \dim(\mathcal{N}) = \dim(\mathcal{E})$ is satisfied. Now define the function

$$\phi\left(\mathbf{X}, \begin{pmatrix} \alpha \\ \beta \end{pmatrix}\right) = \begin{pmatrix} \begin{pmatrix} \alpha\beta & 0 & 0 \\ 0 & \alpha\beta & 0 \\ \mathbf{0} & \mathbf{0} & \beta \end{pmatrix} \mathbf{x}_1 \\ \beta \mathbf{x}_2 \\ \beta \mathbf{x}_3 \end{pmatrix}.$$

Note that for any $\mathbf{X} \in \mathcal{M}$, we have $\phi\left(\mathbf{X}, \begin{pmatrix} 1 \\ 1 \end{pmatrix}\right) = \mathbf{X}$ as mandated by Theorem 2. In addition, the smoothness of the function ϕ directly derives from its definition as it involves only products. Now let \mathbf{Z} be an arbitrary matrix in \mathcal{E}^* . From the expression of ϕ , it can easily be seen that the first term of the inverse $\pi_1(\phi^{-1})$ can be written as

$$\begin{pmatrix} \mathbf{x}_1 \\ \mathbf{x}_2 \\ \mathbf{x}_3 \end{pmatrix} = \lambda \begin{pmatrix} \begin{pmatrix} \gamma & 0 & 0 \\ 0 & \gamma & 0 \\ 0 & 0 & 1 \end{pmatrix} \mathbf{z}_1 \\ \mathbf{z}_2 \\ \mathbf{z}_3 \end{pmatrix}$$

for some λ and γ functions of \mathbf{Z} . Therefore, the inverse of the first component is smooth. Consider the transformation

$\mathbf{u}_1 = \begin{pmatrix} \gamma & 0 & 0 \\ 0 & \gamma & 0 \\ 0 & 0 & 1 \end{pmatrix} \mathbf{z}_1$, $\mathbf{u}_2 = \mathbf{z}_2$, and $\mathbf{u}_3 = \mathbf{z}_3$. If \mathbf{z}_1 is not the zero vector, it is easy to see that there exists a unique γ such that the equality $(\mathbf{u}_1 - \mathbf{u}_2)^T(\mathbf{u}_2 - \mathbf{u}_3) = -(\mathbf{u}_1 - \mathbf{u}_3)^T(\mathbf{u}_2 - \mathbf{u}_3)$

is satisfied. The expression of γ is given by

$$\gamma = \frac{(\mathbf{z}_2 + \mathbf{z}_3)^T(\mathbf{z}_2 - \mathbf{z}_3) - 2\mathbf{z}_1^T(\mathbf{z}_2 - \mathbf{z}_3)}{2\mathbf{z}_1^T \begin{pmatrix} 1 & 0 & 0 \\ 0 & 1 & 0 \\ 0 & 0 & 0 \end{pmatrix} (\mathbf{z}_2 - \mathbf{z}_3)} + 1.$$

If \mathbf{z}_1 is the zero vector then γ can take any real value. Finally, the point $\mathbf{X} \in \mathcal{M}$ is obtained by scaling the matrix \mathbf{U} by the quantity $\lambda = \sqrt{\frac{d^2 \cos(\frac{\pi}{3})}{(\mathbf{u}_1 - \mathbf{u}_3)^T(\mathbf{u}_2 - \mathbf{u}_3)}}$, i.e., $\mathbf{X} = \lambda \mathbf{U}$ to obtain the manifold characterization

$$(\mathbf{x}_1 - \mathbf{x}_2)^T(\mathbf{x}_2 - \mathbf{x}_3) = -d^2 \cos\left(\frac{\pi}{3}\right)$$

$$(\mathbf{x}_1 - \mathbf{x}_3)^T(\mathbf{x}_2 - \mathbf{x}_3) = d^2 \cos\left(\frac{\pi}{3}\right).$$

Since the expressions of γ and λ are rational functions of the argument \mathbf{Z} without any pole as $\mathbf{z}_2 \neq \pm \mathbf{z}_3$ and that \mathbf{X} is obtained by a simple multiplication, it can be concluded that ϕ^{-1} is smooth which gives that ϕ is a diffeomorphism as requested by Theorem 2. Finally, combining all the results above and letting $\mathbf{Z} = \mathbf{X} + \xi_{\mathbf{X}}$, this manuscript proposes the following retraction

$$R_{\mathbf{X}}(\xi_{\mathbf{X}}) = \sqrt{\frac{d^2 \cos(\frac{\pi}{3})}{\lambda}} \begin{pmatrix} \begin{pmatrix} \gamma & 0 & 0 \\ 0 & \gamma & 0 \\ 0 & 0 & 1 \end{pmatrix} \mathbf{z}_1 \\ \mathbf{z}_2 \\ \mathbf{z}_3 \end{pmatrix} \quad (17)$$

with

$$\lambda = \left(\begin{pmatrix} \gamma & 0 & 0 \\ 0 & \gamma & 0 \\ 0 & 0 & 1 \end{pmatrix} \mathbf{z}_1 - \mathbf{z}_3 \right)^T (\mathbf{z}_2 - \mathbf{z}_3)$$

$$\gamma = \begin{cases} \frac{(\mathbf{z}_2 + \mathbf{z}_3)^T(\mathbf{z}_2 - \mathbf{z}_3) - 2\mathbf{z}_1^T(\mathbf{z}_2 - \mathbf{z}_3)}{2\mathbf{z}_1^T \begin{pmatrix} 1 & 0 & 0 \\ 0 & 1 & 0 \\ 0 & 0 & 0 \end{pmatrix} (\mathbf{z}_2 - \mathbf{z}_3)} + 1, & \text{for } \mathbf{z}_1 \neq \mathbf{0} \\ \text{any real value} & \text{for } \mathbf{z}_1 = \mathbf{0}. \end{cases} \quad (18)$$

VI. HIGH ACCURACY 3D LOCATION ESTIMATION

This section exploits the previous results to design a high accuracy spatial location estimation method using ultrasound waves and the fixed geometry of the transmitters. Given the non-convex nature of the problem, Section VI-A presents two types of initialization; a random initialization on the manifold and an improved initialization through the use of a non-linear least squares solver and the Riemannian geometry of the manifold. Section VI-B adapts the template of Riemannian optimization method to the steepest descent algorithm on the equilateral triangle manifold. Finally, Section VIII combines the obtained initialization with the proposed Riemannian optimization algorithm to efficiently solve the 3D spatial location problem of interest in this paper.

A. Initialization and Estimation Accuracy

Incorporating the geometry of the receivers in the optimization problem turns the problem into a non-convex program. While the performance of the proposed Riemannian

optimization algorithm is slightly affected by the choice of the initial point, the performance of some of the benchmark non-convex solvers, that we will compare against, heavily relies on the quality of the initialization. Therefore, we evaluate the performance of the proposed algorithm against the benchmark algorithms using two methods for initialization; a random initialization and an improved initialization. A random initialization on the manifold can be obtained by generating a random orthonormal matrix $\mathbf{O} \in \mathbb{R}^{3 \times 3}$, i.e., $\mathbf{O}\mathbf{O}^T = \mathbf{I}$, and initializing $\mathbf{X} = d\sqrt{\cos(\frac{\pi}{3})}\mathbf{O}$. However, due to the non-convex nature of the optimization problem, better results can be obtained by using an improved initialization.

This section proposes finding an improved initialization by solving the location problem without constraints on the geometry of the transmitters. This can be accomplished using a classical non-linear least squares solver, such as the Gauss-Newton algorithm [18]. Let $\tilde{\mathbf{X}}_0$ be the solution obtained without constraints on the geometry of the transmitters. Such a solution does not necessarily belong to the equilateral triangle manifold. Therefore, the second step in deriving an improved initialization is to “project” the point $\tilde{\mathbf{X}}_0$ to the manifold. This is accomplished by solving the optimization problem

$$\mathbf{X}_0 = \arg \min_{\mathbf{X} \in \mathcal{M}} \|\mathbf{X} - \tilde{\mathbf{X}}_0\|_2^2 \quad (19)$$

The optimization problem in (19) can be efficiently solved using the geometry derived in Section V. Indeed, as pointed out previously, the proposed framework allows to optimize any objective function over the equilateral triangle manifold, including the function $\|\mathbf{X} - \tilde{\mathbf{X}}_0\|_2^2$. Random initialization on the manifold, as described above, can be used to solve (19). The steps of the algorithm are omitted herein as they are provided and described in the next subsection.

Note that the initialization strongly depends on the assumptions on the system and the considered loss function. In other words, while the proposed initialization in (19) performs well for the considered ℓ_2 loss in (4), it might not be optimal for different objective functions.

B. Optimization Over the Equilateral Triangle Manifold

The algorithm starts by initialization $\mathbf{X} = \mathbf{X}_0 \in \mathcal{M}$. Afterwards, the algorithm iterates between finding a search direction and updating the current position. As stated in Section IV, the search direction is given by $\xi_{\mathbf{X}} = -\frac{\overline{\nabla}_{\mathbf{X}} f}{\|\overline{\nabla}_{\mathbf{X}} f\|_{\mathbf{X}}}$ wherein the Riemannian gradient is computed according to (14). The step size t is chosen by backtracking so as it satisfies the following Wolfe conditions [37]

- 1) $f(\mathbf{X} + t\xi_{\mathbf{X}}) \leq f(\mathbf{X}) + c_1 t \xi_{\mathbf{X}}^T \nabla_{\mathbf{X}} f$
- 2) $-\xi_{\mathbf{X}}^T \nabla_{\mathbf{X} + t\xi_{\mathbf{X}}} \leq -c_2 \xi_{\mathbf{X}}^T \nabla_{\mathbf{X}} f$,

for some constants $0 < c_1 < c_2 < 1$. The tangent vector $\xi_{\mathbf{X}}$ scaled with the step size t are retracted to the manifold using (17) to update the position \mathbf{X} . The process is repeated until convergence which can be attested by the norm of the Riemannian gradient. The steps of the proposed Riemannian steepest descent algorithm are summarized in Algorithm 3.

Under the notion of convexity in the Euclidean space, it is worth noting that unlike other non-convex methods, whose complexity is at least quadratic in the number of variables n ,

Algorithm 3 Riemannian Steepest Descent on the Equilateral Triangle Manifold for High Accuracy Location Estimation

Require: Length $d > 0$, initialization \mathbf{X}_0 , a tolerance $\epsilon > 0$, and a smooth function f .

- 1: Initialize $\mathbf{X} = \mathbf{X}_0 \in \mathcal{M}$.
- 2: **while** $\|\overline{\nabla}_{\mathbf{X}} f\|_{\mathbf{X}} \neq \epsilon$ **do**
- 3: Find α and β by solving (15)
- 4: Compute the Riemannian gradient using (14)
- 5: Set search direction $\xi_{\mathbf{X}} = -\frac{\overline{\nabla}_{\mathbf{X}} f}{\|\overline{\nabla}_{\mathbf{X}} f\|_{\mathbf{X}}}$
- 6: Compute the step size t using backtracking.
- 7: Define $\mathbf{Z} = \mathbf{X} + t\xi_{\mathbf{X}}$ and compute γ using (18)
- 8: Define the equilateral triangle \mathbf{U} by

$$[\mathbf{u}_1, \mathbf{u}_2, \mathbf{u}_3] = \left[\begin{array}{ccc} \left(\begin{array}{ccc} \gamma & 0 & 0 \\ 0 & \gamma & 0 \\ 0 & 0 & 1 \end{array} \right) \mathbf{z}_1, \mathbf{z}_2, \mathbf{z}_3 \end{array} \right]$$

- 9: Scale the sides of \mathbf{U} to obtain a triangle in \mathcal{M} by

$$\mathbf{X} = \sqrt{\frac{d^2 \cos(\frac{\pi}{3})}{(\mathbf{u}_1 - \mathbf{u}_3)^T (\mathbf{u}_2 - \mathbf{u}_3)}} \mathbf{U}$$

- 10: **end while**
-

all the steps in our proposed Riemannian method are linear in n . This results in an overall algorithm with linear complexity. Furthermore, recall that Newton’s method on the equilateral triangle manifold is obtained by choosing the tangent vector that solves $\overline{\nabla}_{\mathbf{X}}^2 f[\xi_{\mathbf{X}}] = -\overline{\nabla}_{\mathbf{X}} f$. Since the previous step can be accomplished in n^2 operations, our proposed Riemannian Newton’s method is quadratic in the number of variables which competes with the complexity of first-order generic non-convex solvers, e.g., interior points method (IPM).

VII. CONSTRAINED CRAMÉR RAO BOUND

The Cramér Rao bound (CRB) matrix provides a lower bound on the covariance matrix of any unbiased estimator. In some applications, such as the one in this paper, the parameters that we intend to estimate are constrained. To address this problem, several versions of the CRB have been derived for constrained parameter estimation [38], [39]. While the approach by Smith in [39] extends the theory of CRB to parameters on manifold, the steps required to derive the constrained CRB are a bit more complicated than the approach in [40]. In this section, we derive the CRBs under parametric constraints for our setup using the simpler approach based on [40]. To start with, we derive the unconstrained CRBs for our estimation problem. Then, we utilize these bounds in the constrained CRB (CCRB) theorem [40] to derive the constrained CRB.

A. The unconstrained CRB

Let the received signal from the i^{th} transmitter at the j^{th} receiver be given by [30]

$$\zeta_{ij}(t) = \psi_{ij} s_i(t - \kappa_{ij}) + n_{ij}(t), \quad i = 1, 2, \dots, M, \quad j = 1, 2, \dots, N, \quad (20)$$

where ψ_{ij} is an attenuation factor incurred by propagation, $s_i(t)$ is the passband transmitted signal from the i^{th} transmitter,

κ_{ij} is the time of flight (TOF) from the i^{th} transmitter to the j^{th} receiver, M is the number of transmitters, N is the number of receivers, and $n_{ij}(t)$ is an additive Gaussian noise with zero mean and variance σ_{ij}^2 . Let the complex envelope of the received signal be $\zeta_{e_{ij}}(t)$ which can be obtained using an IQ demodulator. We obtain the discrete-time version of this envelope by sampling $\zeta_{e_{ij}}(t)$ at a sampling period T_s , which gives

$$\zeta_{e_{ij}}[k] = \psi_{ij} s_{e_i}[k - \tau_{ij}] + n_{ij}[k], \quad (21)$$

where $s_{e_i}[k]$ is the discrete-time complex envelope of the transmitted signal from the i^{th} transmitter, τ_{ij} is the TOF, κ_{ij} , normalized by T_s and rounded to the nearest integer, $n_{ij}[k]$ is a discrete-time complex additive Gaussian noise with zero mean and variance σ_{ij}^2 . Under a very high sampling rate, we assume that the error due to rounding is negligible. The $n_{ij}[k]$'s are assumed to be independent, consequently the received signals $\zeta_{e_{ij}}[k]$ are independent. The time of flight τ_{ij} is given by

$$\tau_{ij} = \frac{\|\mathbf{x}_i - \mathbf{b}_j\|_2}{cT_s}, \quad (22)$$

where \mathbf{x}_i is the unknown 3D location of the i^{th} transmitter, \mathbf{b}_j is the known 3D location of the j^{th} receiver, and c is the speed of sound. Therefore, the discrete-time complex envelope of the received signal can be re-written as

$$\zeta_{e_{ij}}[k] = \psi_{ij} s_{e_i}\left[k - \frac{\|\mathbf{x}_i - \mathbf{b}_j\|_2}{cT_s}\right] + n_{ij}[k]. \quad (23)$$

In our setup, we have three transmitters and four receivers, hence $M = 3$ and $N = 4$. Let the complex envelope of the transmitted signal $s_{e_i}[k]$ be a Zadoff-Chu sequence [41] of length K which is given by

$$s_{e_i}[k] = e^{j\phi_i[k]}, \quad (24)$$

where $\phi_i[k]$ is given by

$$\phi_i[k] = \begin{cases} \frac{\pi R_i}{K} k(k+1) & \text{if } K \text{ is odd} \\ \frac{\pi R_i}{K} k^2 & \text{if } K \text{ is even,} \end{cases}$$

where R_i and K are coprime. The attenuation factors ψ_{ij} are deterministic and assumed to be constant over the observation interval. Therefore, they will appear as scaling factors on the maximum likelihood estimator. The probability of a received symbol $\zeta_{e_{ij}}[k]$ conditional on $\boldsymbol{\theta}$, where $\boldsymbol{\theta} = [\mathbf{x}_1, \mathbf{x}_2, \mathbf{x}_3]^T$, is given by

$$p(\zeta_{e_{ij}}[k]|\boldsymbol{\theta}) = \frac{1}{\pi\sigma_{ij}^2} e^{-\frac{1}{\sigma_{ij}^2} |\zeta_{e_{ij}}[k] - \psi_{ij} s_{e_i}[k - \frac{\|\mathbf{x}_i - \mathbf{b}_j\|_2}{cT_s}]|^2}. \quad (25)$$

The noise samples $n_{ij}[k]$'s are independent, hence the probability of the received sequence can be expressed as

$$p(\boldsymbol{\zeta}_{e_{ij}}|\boldsymbol{\theta}) = \prod_{k=0}^{K-1} p(\zeta_{e_{ij}}[k]|\boldsymbol{\theta}). \quad (26)$$

By taking the natural logarithm of this probability distribution function and expanding the terms inside the summation, the log-likelihood of the received signal can be written as

$$\begin{aligned} \ln p(\boldsymbol{\zeta}_{e_{ij}}|\boldsymbol{\theta}) &= -K \ln(\pi\sigma_{ij}^2) - \frac{1}{\sigma_{ij}^2} \sum_{k=0}^{K-1} \left[|\zeta_{e_{ij}}[k]|^2 + |\psi_{ij} s_{e_i}[k - \frac{\|\mathbf{x}_i - \mathbf{b}_j\|_2}{cT_s}]|^2 \right. \\ &\quad \left. - \zeta_{e_{ij}}^*[k] \psi_{ij} s_{e_i}[k - \frac{\|\mathbf{x}_i - \mathbf{b}_j\|_2}{cT_s}] - \zeta_{e_{ij}}[k] \psi_{ij} s_{e_i}^*[k - \frac{\|\mathbf{x}_i - \mathbf{b}_j\|_2}{cT_s}] \right]. \end{aligned}$$

Since the $\zeta_{e_{ij}}$'s are independent, the log-likelihood function can be expressed as

$$\ln p(\boldsymbol{\zeta}|\boldsymbol{\theta}) = \sum_{i=1}^M \sum_{j=1}^N \ln p(\boldsymbol{\zeta}_{e_{ij}}|\boldsymbol{\theta}). \quad (27)$$

We can write the log-likelihood of the received signal as

$$\begin{aligned} L(\mathbf{x}_1, \mathbf{x}_2, \mathbf{x}_3) &= -K \sum_{i=1}^M \sum_{j=1}^N \ln(\pi\sigma_{ij}^2) - \sum_{i=1}^M \sum_{j=1}^N \frac{1}{\sigma_{ij}^2} \left[\sum_{k=0}^{K-1} \left[|\zeta_{e_{ij}}[k]|^2 + \right. \right. \\ &\quad \left. \left. |\psi_{ij} s_{e_i}[k - \frac{\|\mathbf{x}_i - \mathbf{b}_j\|_2}{cT_s}]|^2 - \zeta_{e_{ij}}^*[k] \psi_{ij} s_{e_i}[k - \frac{\|\mathbf{x}_i - \mathbf{b}_j\|_2}{cT_s}] - \zeta_{e_{ij}}[k] \psi_{ij} s_{e_i}^*[k - \frac{\|\mathbf{x}_i - \mathbf{b}_j\|_2}{cT_s}] \right] \right]. \end{aligned}$$

Substitute $s_{e_i}[k] = e^{j\phi_i[k]}$ to obtain

$$\begin{aligned} L(\mathbf{x}_1, \mathbf{x}_2, \mathbf{x}_3) &= -K \sum_{i=1}^M \sum_{j=1}^N \left[\ln(\pi\sigma_{ij}^2) - \frac{\psi_{ij}^2}{\sigma_{ij}^2} \right] - \sum_{i=1}^M \sum_{j=1}^N \frac{1}{\sigma_{ij}^2} \left[\sum_{k=0}^{K-1} \right. \\ &\quad \left. \left[|\zeta_{e_{ij}}[k]|^2 - \zeta_{e_{ij}}^*[k] \psi_{ij} e^{j\phi_i[k - \frac{\|\mathbf{x}_i - \mathbf{b}_j\|_2}{cT_s}]} - \zeta_{e_{ij}}[k] \psi_{ij} e^{-j\phi_i[k - \frac{\|\mathbf{x}_i - \mathbf{b}_j\|_2}{cT_s}]} \right] \right]. \end{aligned}$$

The unconstrained Fisher information matrix (FIM) for $\mathbf{x}_1, \mathbf{x}_2$, and \mathbf{x}_3 is given by $J_{ij} = -\mathbb{E}\left[\frac{\partial^2 L}{\partial \mathbf{x}_i \partial \mathbf{x}_j}\right]$ [42]. Since $\mathbb{E}\left[\frac{\partial^2 L}{\partial \mathbf{x}_i \partial \mathbf{x}_j}\right] = \mathbf{0}_{3 \times 3}$, $\forall i \neq j$, the unconstrained FIM can be written as

$$\mathbf{J} = - \begin{bmatrix} \mathbb{E}[\mathbf{H}^1] & \mathbf{0}_{3 \times 3} & \mathbf{0}_{3 \times 3} \\ \mathbf{0}_{3 \times 3} & \mathbb{E}[\mathbf{H}^2] & \mathbf{0}_{3 \times 3} \\ \mathbf{0}_{3 \times 3} & \mathbf{0}_{3 \times 3} & \mathbb{E}[\mathbf{H}^3] \end{bmatrix},$$

where $\mathbb{E}[\mathbf{H}^i] = \mathbb{E}\left[\frac{\partial^2 L}{\partial \mathbf{x}_i \partial \mathbf{x}_i}\right] = -\mathbb{E}\left[\left(\frac{\partial L}{\partial \mathbf{x}_i}\right)\left(\frac{\partial L}{\partial \mathbf{x}_i}\right)^T\right]$. With simple algebraic manipulations we obtain the following expression $\mathbb{E}[\mathbf{H}^i] = \sum_{j=1}^N \frac{-2\psi_{ij}^2}{\sigma_{ij}^2} \sum_{k=0}^{K-1} \left(\nabla_{\mathbf{x}_i} \phi_i\left[k - \frac{\|\mathbf{x}_i - \mathbf{b}_j\|_2}{cT_s}\right]\right) \left(\nabla_{\mathbf{x}_i} \phi_i\left[k - \frac{\|\mathbf{x}_i - \mathbf{b}_j\|_2}{cT_s}\right]\right)^T$, (29)

where $\phi_i[k]$ is given by (24) and $\nabla_{\mathbf{x}_i}$ is the gradient with respect to \mathbf{x}_i . For an even-length sequence, the Hessian matrix can be written in the following expression using sum identities on k and k^2

$$\begin{aligned} \mathbb{E}[\mathbf{H}^i] &= \sum_{j=1}^N -8 \left(\frac{\psi_{ij} \pi R_i}{\sigma_{ij} K c T_s}\right)^2 \left[\frac{K}{c^2 T_s^2} - \frac{K(K-1)}{c T_s \|\mathbf{x}_i - \mathbf{b}_j\|_2} + \right. \\ &\quad \left. \frac{K(K-1)(2K-1)}{6 \|\mathbf{x}_i - \mathbf{b}_j\|_2^2} \right] (\mathbf{x}_i - \mathbf{b}_j)(\mathbf{x}_i - \mathbf{b}_j)^T. \end{aligned}$$

Similarly, for an odd-length sequence, the expectation of the Hessian matrix is given by

$$\begin{aligned} \mathbb{E}[\mathbf{H}^i] &= \sum_{j=1}^N -2 \left(\frac{\psi_{ij} \pi R_i}{\sigma_{ij} K c T_s}\right)^2 \left[\frac{4K}{c^2 T_s^2} - \frac{4K^2}{c T_s \|\mathbf{x}_i - \mathbf{b}_j\|_2} + \right. \\ &\quad \left. \frac{K(2K-1)(2K+1)}{3 \|\mathbf{x}_i - \mathbf{b}_j\|_2^2} \right] (\mathbf{x}_i - \mathbf{b}_j)(\mathbf{x}_i - \mathbf{b}_j)^T. \end{aligned}$$

If the FIM \mathbf{J} is nonsingular, the unconstrained CRBs are given

by [42]

$$CRB \geq \mathbf{J}^{-1}. \quad (30)$$

In the next section, we utilize the unconstrained FIM to obtain the constrained CRBs.

B. The constrained CRB

This section provides the CRB for estimating the 3D position of the three transmitters under the equilateral triangle constraints (7), which can be reformulated as

$$\mathbf{q}(\mathbf{x}_1, \mathbf{x}_2, \mathbf{x}_3) = \begin{bmatrix} \|\mathbf{x}_1 - \mathbf{x}_2\|^2 - d^2 \\ \|\mathbf{x}_2 - \mathbf{x}_3\|^2 - d^2 \\ \|\mathbf{x}_3 - \mathbf{x}_1\|^2 - d^2 \end{bmatrix} = \mathbf{0}. \quad (31)$$

The three constraints given by (31) are continuously differentiable. Let us denote the vector that we would like to estimate by $\boldsymbol{\theta} = [\mathbf{x}_1, \mathbf{x}_2, \mathbf{x}_3]^T \in \mathbb{R}^{9 \times 1}$. Moreover, let the 3×9 Jacobian matrix of the constraints be defined as

$$\mathbf{Q}(\boldsymbol{\theta}) = \frac{\partial \mathbf{q}}{\partial \boldsymbol{\theta}} = 2 \begin{bmatrix} (\mathbf{x}_1 - \mathbf{x}_2)^T & -(\mathbf{x}_1 - \mathbf{x}_2)^T & \mathbf{0}^T \\ \mathbf{0}^T & (\mathbf{x}_2 - \mathbf{x}_3)^T & -(\mathbf{x}_2 - \mathbf{x}_3)^T \\ -(\mathbf{x}_3 - \mathbf{x}_1)^T & \mathbf{0}^T & (\mathbf{x}_3 - \mathbf{x}_1)^T \end{bmatrix}. \quad (32)$$

Since there are no redundant constraints in (31), the matrix $\mathbf{Q}(\boldsymbol{\theta})$ is full row rank for any given $\boldsymbol{\theta}$. Therefore, there exists a matrix $\boldsymbol{\Psi} \in \mathbb{R}^{9 \times 6}$ whose columns form an orthonormal basis for the null space of $\mathbf{Q}(\boldsymbol{\theta})$ [40], that is

$$\mathbf{Q}(\boldsymbol{\theta})\boldsymbol{\Psi} = \mathbf{0}, \quad (33)$$

where $\boldsymbol{\Psi}^T\boldsymbol{\Psi} = \mathbf{I}$. We can re-write the Jacobian matrix of the constraints into the following format

$$\mathbf{Q}(\boldsymbol{\theta}) = \begin{bmatrix} a_1 & a_2 & a_3 & -a_1 & -a_2 & -a_3 & 0 & 0 & 0 \\ 0 & 0 & 0 & b_1 & b_2 & b_3 & -b_1 & -b_2 & -b_3 \\ -c_1 & -c_2 & -c_3 & 0 & 0 & 0 & c_1 & c_2 & c_3 \end{bmatrix}, \quad (34)$$

where $(\mathbf{x}_1 - \mathbf{x}_2)^T = [a_1, a_2, a_3]$, $(\mathbf{x}_2 - \mathbf{x}_3)^T = [b_1, b_2, b_3]$ and $(\mathbf{x}_3 - \mathbf{x}_1)^T = [c_1, c_2, c_3]$. The null space is given by (28).

To derive the constrained CRB, this section utilizes the constrained CRB theorem [40] which can be written as

Theorem 3. *Let $\hat{\boldsymbol{\theta}}$ be an unbiased estimate of $\boldsymbol{\theta}$ satisfying (31) and let $\boldsymbol{\Psi}$ be as defined in (33). If $\boldsymbol{\Psi}^T\mathbf{J}\boldsymbol{\Psi}$ is nonsingular, then the constrained CRB is given by*

$$CCRB \geq \boldsymbol{\Psi}(\boldsymbol{\Psi}^T\mathbf{J}\boldsymbol{\Psi})^{-1}\boldsymbol{\Psi}^T. \quad (35)$$

We numerically evaluate the CCRB, given by (35), under different SNR scenarios and compare the performance of our algorithm against these bounds in the Results section.

VIII. RESULTS

This section presents the simulation results to evaluate the proposed algorithm in a noisy environment. The first subsection presents the simulation environment and parameters. The

second subsection evaluates the performance of the proposed algorithm against the benchmark methods, namely the interior point method (IPM) [43]–[45], the active set algorithm [46], and the sequential quadratic programming (SQP) algorithm [46]. Moreover, the paper illustrates the improvement in the location estimation accuracy as compared to the commonly used trilateration algorithm which utilizes Gauss-Newton (GN) method [26].

Besides the previously mentioned steepest descent and Newton's algorithms on manifolds, this paper implements the Riemannian version of the trust region method [32], [47]. These methods can readily be implemented using the derived geometry in Section V. Indeed, while these algorithms require a vector transport \mathcal{T} , the expression of such operator can be obtained by exploiting the linear structure of the embedding space as $\mathcal{T}_{\eta\mathbf{x}}(\xi\mathbf{x}) = \Pi_{\mathbb{R}\mathbf{x}}(\eta\mathbf{x})(\xi\mathbf{x})$ (see Proposition 8.1.2 [35]). All methods use the same initial point which is obtained using one of two methods; (1) random initialization on the manifold, or (2) the GN-based trilateration method and projecting it onto the equilateral triangle manifold.

All Riemannian algorithms are implemented using the Matlab toolbox Manopt [48] on an Intel Core i5 (2.7 GHz) computer with 8Gb 2.4 GHz DDR3 RAM. In these simulations, the maximum number of iterations is set to 1000, the optimality tolerance is set to 10^{-10} , and the step tolerance is set to 10^{-16} . All the benchmark methods are implemented using MATLAB built-in solvers, which are computationally efficient.

A. Simulation Setup

The size of the room, where the target is located, is given by 4 m x 4 m x 3 m. To evaluate the CRB and CCRB, the three transmitters are fixed to a certain location [2, 2, 1]m, [2.1, 2, 1]m and [2.05, 2, 1.0866]m. The length of the sides of the equilateral triangle, d , is chosen to be 10 cm, unless otherwise indicated. The true ranges from transmitters to beacons, denoted by the κ_{ij} 's, are computed. Three different Zadoff-Chu sequences, with a length of 151 symbols, are assigned to each of the three transmitters. The received signal consists of a delayed version of the transmitted signal and additive Gaussian noise with zero mean and variance σ_{ij}^2 . The distances between the transmitters and receivers can be estimated using the algorithm in our previous work [17].

The noisy range estimates \hat{d}_{ij} are utilized in the GN-based trilateration algorithm to obtain initial estimates of the transmitters locations. These initial locations are projected onto the equilateral triangles manifold by solving (19) to

$$\boldsymbol{\Psi} = \text{NULL}(\mathbf{Q}) = \begin{bmatrix} a_3c_2 - a_2c_3 & c_2(a_1b_2 - a_2b_1) & c_2(a_1b_3 - a_3b_1) & 1 & c_2(a_2b_1 - a_1b_2) & a_2b_1c_3 - a_1b_3c_2 \\ a_1c_3 - a_3c_1 & c_1(a_2b_1 - a_1b_2) & c_1(a_3b_1 - a_1b_3) & 0 & a_1(b_2c_1 - b_1c_2) & a_1(b_3c_1 - b_1c_3) \\ a_2c_1 - a_1c_2 & 0 & 0 & 0 & 0 & 0 \\ 0 & b_2(a_1c_2 - a_2c_1) & b_3(a_1c_2 - a_2c_1) & 1 & b_2(a_2c_1 - a_1c_2) & b_3(a_2c_1 - a_1c_2) \\ 0 & b_1(a_2c_1 - a_1c_2) & 0 & 0 & 0 & 0 \\ 0 & 0 & b_1(a_2c_1 - a_1c_2) & 0 & 0 & 0 \\ 0 & 0 & 0 & 1 & 0 & 0 \\ 0 & 0 & 0 & 0 & b_1(a_2c_1 - a_1c_2) & 0 \\ 0 & 0 & 0 & 0 & 0 & b_1(a_2c_1 - a_1c_2) \end{bmatrix}. \quad (28)$$

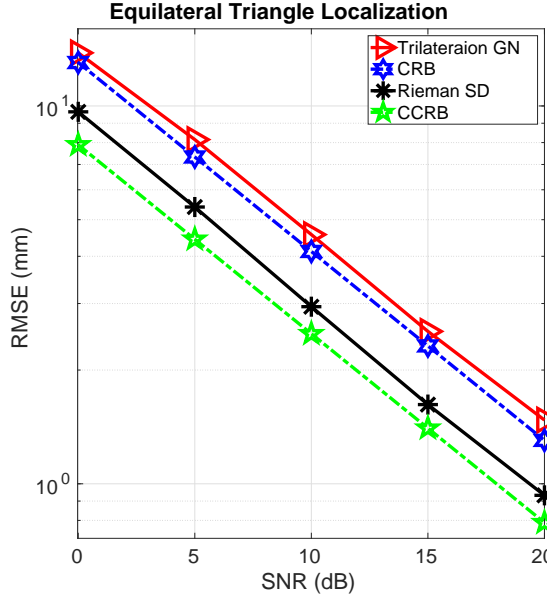


Fig. 2: RMSE vs SNR.

obtain an initial point that belongs to the manifold. For each SNR scenario, 1000 observations are processed.

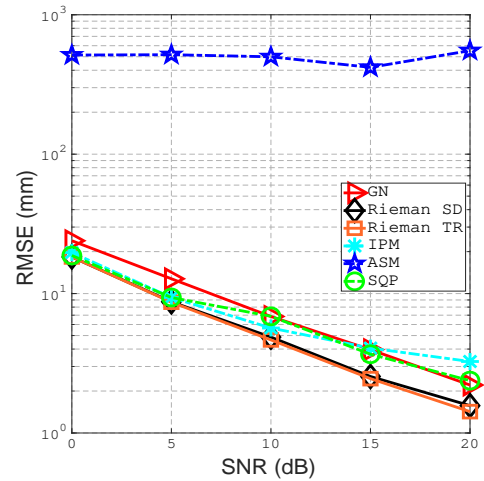
The performance of the proposed algorithm is evaluated by comparing the root mean square error (RMSE) calculated as the square root of the average mean square error between the genuine transmitters' positions and their estimates. Furthermore, the computational complexity for the proposed algorithm is compared against the considered benchmark algorithms by calculating the overall running time required to obtain an estimate of the target position.

B. Numerical Results

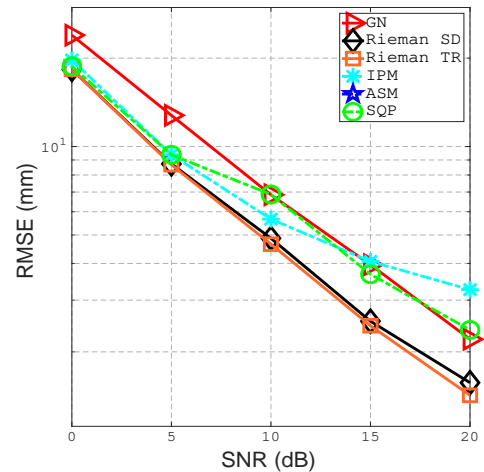
We illustrate the localization accuracy improvement, that we obtain through exploiting the equilateral triangle geometry, by evaluating the CRB and the constrained CRB. Figure 2 plots the RMSE for the GN-based trilateration and the proposed algorithm against the square root of the CRB and the constrained CRB. This plot shows the improvement in the localization accuracy as the constrained CRB is lower than the unconstrained CRB. Moreover, the proposed algorithm has an RMSE lower than the unconstrained Gauss-Newton method as expected. Furthermore, we would like to highlight that the accuracy of the localization algorithm is affected by the accuracy of the ranging algorithm. Consequently, the localization algorithm can be further improved by utilizing a more accurate ranging algorithm to estimate the distances between the transmitters and the receivers. Finally, using the maximum likelihood estimator instead of the nonlinear least squares as a cost function might give an RMSE tighter to the CRB and CCRB.

Figure 3 shows the RMSE for the proposed algorithm against the benchmark algorithms using random initialization. In this simulation, all algorithms iterate until they converge or the number of iterations exceed a threshold, which is set to 10000 iterations to guarantee that no method stop

due to being slow. Both Riemannian algorithms, trust region [32], [47] and steepest descent-based, given by Algorithm 3, outperforms the benchmark algorithms. Moreover, we notice that the constrained ASM method does not always converge when using random initialization, hence it gives a very high RMSE. Furthermore, we notice that under low SNR values, the proposed and the state-of-the-art algorithms give a remarkable improvement as compared to the unconstrained GN-based localization algorithm. The proposed Riemannian-based algorithms maintain the considerable improvement in the localization accuracy under all SNR values. On the contrary, while the performance of the benchmark algorithms improves with increasing the SNR values, their improvement is not substantial as compared to the improvement in the proposed Riemannian algorithms and the unconstrained GN-based algorithm. We conclude that under random initialization, it is recommended to use the proposed Riemannian algorithms under all SNR values to obtain more accurate results as compared to the unconstrained GN-based algorithm and the popular generic non-convex solvers.

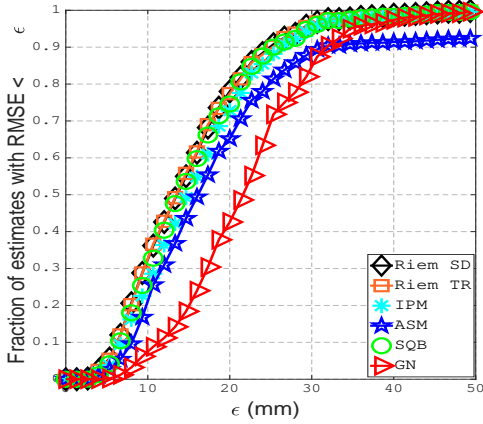


(a) zoomed-out

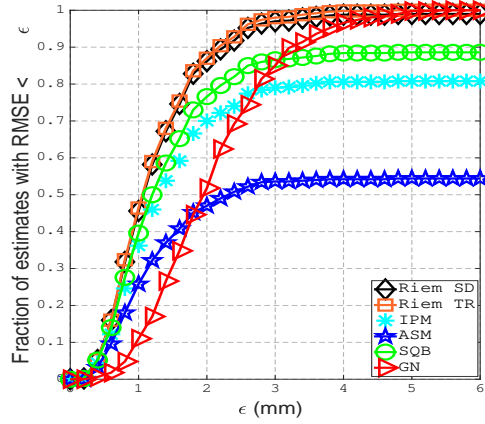


(b) zoomed-in

Fig. 3: RMSE vs SNR with random initialization.



(a) 0 dB SNR.



(b) 20 dB SNR.

Fig. 4: Cumulative RMSE of the three transmitters for various SNR values with random initialization

Figure 4 shows the cumulative error in the estimated location under two SNR scenarios. The cumulative error plots give an insight about the distribution of the error, hence the effect of outliers on our conclusions will be reduced as compared to conclusions based on the plot of the RMSE. The proposed algorithm outperforms the benchmark algorithms under all SNR values. In the 0 dB SNR, more than 90% of the location estimates are in less than 24.8 mm RMSE for the proposed Riemannian algorithm. On the other side, less than 88.5%, 88%, and 79% of the location estimates are in less than 24.8 mm RMSE for the SQP, IPM and ASM method respectively. It is worth noting that while the ASM method has a very high RMSE under 0 dB SNR as shown in Figure 3, its cumulative error is slightly higher than the other benchmark algorithms. This means that the big increase in the RMSE as compared to the other algorithms is due to outliers. In the 20 dB SNR, more than 90% of the location estimates are in less than 2.5 mm RMSE for the proposed Riemannian algorithm. On the other hand, less than 90%, 80%, and 55% of the location estimates are in less than 6 mm RMSE for the SQP, IPM and ASM method respectively.

Since some of the benchmark algorithms are very sensitive to the choice of the initial point, we evaluate the algorithms using an improved initialization, obtained using the algorithm shown in Section VI.A. Figure 5 shows the RMSE for the proposed and benchmark algorithms using improved initialization under computational time threshold. The computational time threshold is set to make sure that all results are obtained under the same running time. As expected, the improved initial point has a lower RMSE compared to the unconstrained GN-based estimate. Moreover, the improvement using the ASM method is marginal when compared to the improved initial point. However, we notice a remarkable improvement when using the IPM and SQP methods as compared to the projected GN method. Lastly, both Riemannian-based localization methods outperform all benchmark algorithms under all SNR scenarios.

Figure 6 shows the cumulative error in the estimated location under two different SNR scenarios using an improved initialization under running time threshold. The proposed

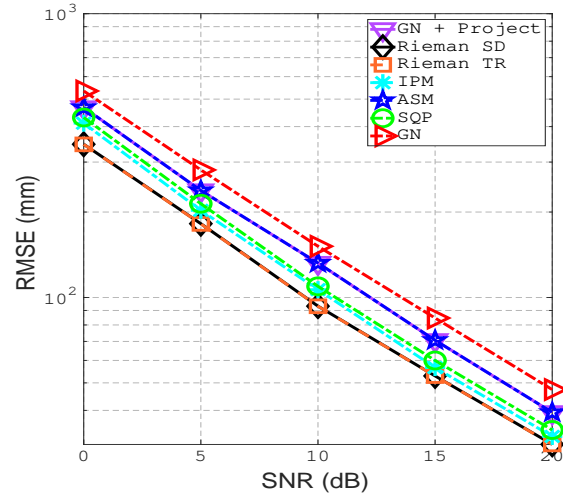
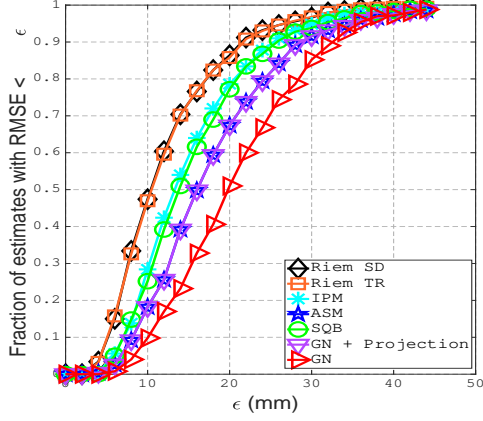


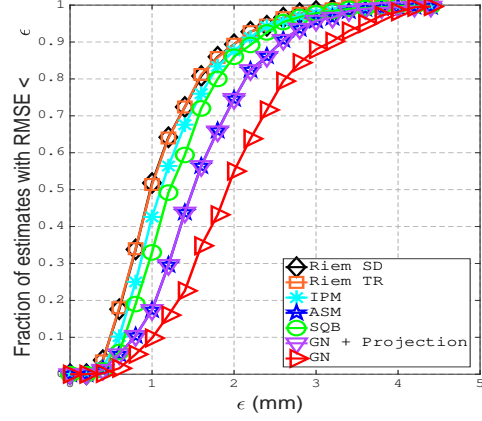
Fig. 5: RMSE vs SNR using improved initialization under running time threshold

algorithm outperforms the benchmark algorithms. In the 0 dB SNR, more than 90 % of the location estimates are in less than 22 mm RMSE for the proposed Riemannian algorithm. On the contrary, less than 90 % of the location estimates are in less than 25 mm, 28 mm, and 25 mm RMSE for the IPM, Active-set method and SQP method, respectively. In the 20 dB SNR, more than 90 % of the location estimates are in less than 2.04 mm RMSE for the proposed Riemannian algorithm. In contrast to the proposed algorithm, less than 90 % of the location estimates are in less than 2.12 mm, 2.55 mm, and 2.25 mm RMSE for the IPM, Active-set method and SQP method, respectively.

We compare the computational complexity of all algorithms by calculating the running time required to reach the minimum of the cost function under different SNR values. Figure 7 shows both the running time and the RMSE for various SNR values using an improved initialization, obtained by projecting the GN solution to the manifold. Figure 7a shows that the trust region Riemannian localization algorithm requires much



(a) 0 dB SNR.



(b) 20 dB SNR.

Fig. 6: Cumulative RMSE of the three transmitters for various SNR values with improved initialization

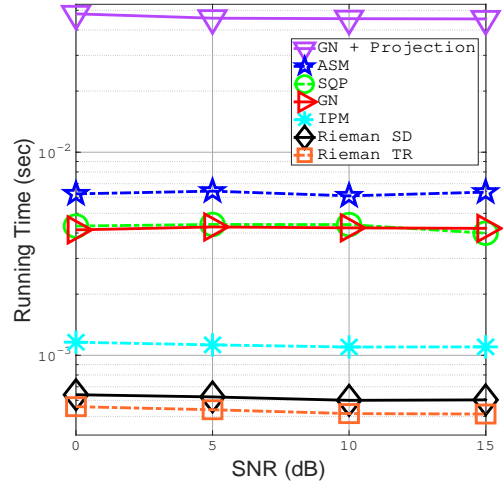
Algorithm	Running Time (msec)			
	0 dB	5 dB	10 dB	15 dB
Projected GN	48.01	45.70	45.45	45.32
ASM	6.237	6.433	6.097	6.360
SQP	4.330	4.409	4.402	3.994
IPM	1.160	1.125	1.099	1.100
Rieman SD	0.640	0.624	0.600	0.603
Rieman TR	0.558	0.539	0.516	0.514

TABLE I: Running time for all algorithms under different SNR values using improved initialization

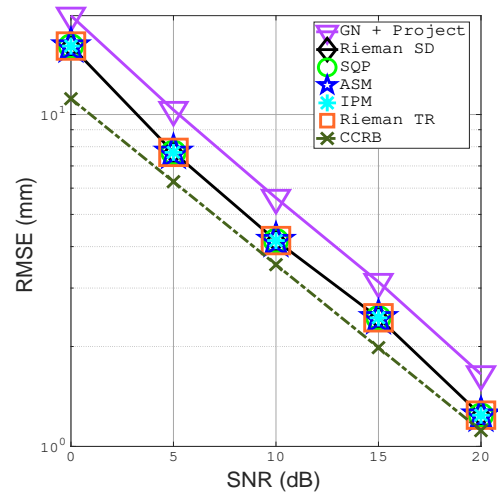
lower running time to reach the minimum compared to all benchmark algorithms. Steepest descent-based Riemannian localization requires more time than the trust region Riemannian method because it has slower convergence rate. Moreover, Figure 7b shows that the constrained localization methods improves the accuracy of the projected GN-based solution. Finally, Table I shows the running time for all algorithms when using improved initialization. The projected GN method, used to obtain an improved initial point, is computationally demanding which increases the overall computational time for all algorithms. Since the proposed Riemannian algorithm has a good performance under random initialization, unlike the benchmark algorithms, this makes the proposed algorithm more practical for indoor localization systems.

IX. CONCLUSION

This paper exploits the fixed geometry of the transmitters to improve the accuracy of the spatial location estimates using ultrasound waves. The transmitters are assumed to be placed on an equilateral triangle, and such information is leveraged in the derivation of a non-convex optimization problem. As the set of feasible solutions admits a Riemannian structure, the manuscript investigates its geometry so as to design efficient optimization algorithms. Simulation results are presented to attest to the superiority of the proposed approach against popular methods from the literature both from a performance and complexity perspectives.



(a) Running time per estimate.



(b) MSE vs SNR.

Fig. 7: Running time and RMSE vs SNR using improved initialization.

As a future research direction, one can investigate the problem of optimizing the geometry for transmitters to maximize the efficiency of the location estimation using ultrasound waves. In the study of the optimal three-transmitter array geometry, we can evaluate the constrained Cramér-Rao bound for triangles with different angles under a fixed triangle area. Moreover, this work can be extended to consider location estimation of a moving target where the accuracy of the estimated distances degrades.

REFERENCES

- [1] P. Davidson and R. Piché, "A survey of selected indoor positioning methods for smartphones," *IEEE Communications Surveys & Tutorials*, vol. 19, no. 2, pp. 1347–1370, 2016.
- [2] Y. Gu, A. Lo, and I. Niemegeers, "A survey of indoor positioning systems for wireless personal networks," *IEEE Communications surveys & tutorials*, vol. 11, no. 1, pp. 13–32, 2009.
- [3] G. Borriello, "Location systems for ubiquitous computing," *IEEE computer*, pp. 57–66, 2000.
- [4] K. Whitehouse, C. Karlof, and D. Culler, "A practical evaluation of radio signal strength for ranging-based localization," *ACM Sigmobile Mobile Computing and Communications Review*, vol. 11, no. 1, pp. 41–52, 2007.
- [5] Ç. Yüzbaşıoğlu and B. Barshan, "Improved range estimation using simple infrared sensors without prior knowledge of surface characteristics," *Measurement Science and Technology*, vol. 16, no. 7, p. 1395, 2005.
- [6] M.-C. Amann, T. M. Bosch, M. Lescure, R. A. Myllyläe, and M. Rioux, "Laser ranging: A critical review of unusual techniques for distance measurement," *Optical engineering*, vol. 40, 2001.
- [7] R. M. Narayanan and M. Dawood, "Doppler estimation using a coherent ultrawide-band random noise radar," *IEEE Transactions on Antennas and Propagation*, vol. 48, no. 6, pp. 868–878, 2000.
- [8] M. Cypriani, F. Lassabe, P. Canalda, and F. Spies, "Open wireless positioning system: A wi-fi-based indoor positioning system," in *Proc. of the 70th IEEE Vehicular Technology Conference Fall (VTC-F'09), Anchorage, Alaska, USA*. IEEE, 2009, pp. 1–5.
- [9] R. H. Rasshofer and K. Gresser, "Automotive radar and lidar systems for next generation driver assistance functions?" *Advances in Radio Science*, vol. 3, 2005.
- [10] F. Ijaz, H. K. Yang, A. W. Ahmad, and C. Lee, "Indoor positioning: A review of indoor ultrasonic positioning systems," in *Proc. of the 15th International Conference on Advanced Communications Technology (ICACT'13), PyeongChang, Korea*. IEEE, 2013, pp. 1146–1150.
- [11] M. Kushwaha, K. Molnar, J. Sallai, P. Volgyesi, M. Maroti, and A. Lédeczi, "Sensor node localization using mobile acoustic beacons," in *Proc. of the IEEE International Conference on Mobile Adhoc and Sensor Systems Conference (MASS'05), Washington, DC, USA*. IEEE, 2005, pp. 9–pp.
- [12] F. Seco, A. R. Jiménez, C. Prieto, J. Roa, and K. Koutsou, "A survey of mathematical methods for indoor localization," in *Proc. of the IEEE International Symposium on Intelligent Signal Processing (WISP'09), Budapest, Hungary*. IEEE, 2009, pp. 9–14.
- [13] F. Zafari, A. Gkelias, and K. K. Leung, "A survey of indoor localization systems and technologies," *IEEE Communications Surveys & Tutorials*, vol. 21, no. 3, pp. 2568–2599, 2019.
- [14] Z. Yang, Z. Zhou, and Y. Liu, "From rssi to csi: Indoor localization via channel response," *ACM Computing Surveys (CSUR)*, vol. 46, no. 2, pp. 1–32, 2013.
- [15] S. Kumar, S. Gil, D. Katabi, and D. Rus, "Accurate indoor localization with zero start-up cost," in *Proc. of the 20th Annual International Conference on Mobile Computing and Networking (MobiCom'14), Maui, Hawaii, USA*, 2014, pp. 483–494.
- [16] R. B. Langley *et al.*, "Dilution of precision," *GPS world*, vol. 10, no. 5, pp. 52–59, 1999.
- [17] M. H. AlSharif, M. Saad, M. Siala, T. Ballal, H. Boujemaa, and T. Y. Al-Naffouri, "Zadoff-chu coded ultrasonic signal for accurate range estimation," in *Proc. of the 25th European Signal Processing Conference (EUSIPCO'17), Kos Island, Greece*. IEEE, 2017, pp. 1250–1254.
- [18] S. Wright and J. Nocedal, "Numerical optimization," *Springer Science*, vol. 35, no. 67-68, p. 7, 1999.
- [19] A. Ward, A. Jones, and A. Hopper, "A new location technique for the active office," *IEEE Personal communications*, vol. 4, no. 5, pp. 42–47, 1997.
- [20] N. B. Priyantha, A. Chakraborty, and H. Balakrishnan, "The cricket location-support system," in *Proc. of the 6th Annual International Conference on Mobile Computing and Networking (MobiCom'00), Boston, Massachusetts, USA*, 2000, pp. 32–43.
- [21] J. Xiong, "Pushing the limits of indoor localization in today's wi-fi networks," Ph.D. dissertation, University College London, 2015.
- [22] Y. Fukujū, M. Minami, H. Morikawa, and T. Aoyama, "Dolphin: An autonomous indoor positioning system in ubiquitous computing environment," in *Proc. of the IEEE Workshop on Software Technologies for Future Embedded Systems (WSTFES'03), Hokkaido, Japan*. IEEE, 2003, pp. 53–56.
- [23] M. M. Saad, C. J. Bleakley, T. Ballal, and S. Dobson, "High-accuracy reference-free ultrasonic location estimation," *IEEE Transactions on Instrumentation and Measurement*, vol. 61, no. 6, pp. 1561–1570, 2012.
- [24] N. Iliiev and I. Paprotny, "Review and comparison of spatial localization methods for low-power wireless sensor networks," *IEEE Sensors Journal*, vol. 15, no. 10, pp. 5971–5987, 2015.
- [25] J. R. Gonzalez and C. J. Bleakley, "High-precision robust broadband ultrasonic location and orientation estimation," *IEEE Journal of selected topics in Signal Processing*, vol. 3, no. 5, pp. 832–844, 2009.
- [26] W. H. Foy, "Position-location solutions by taylor-series estimation," *IEEE Transactions on Aerospace and Electronic Systems*, no. 2, pp. 187–194, 1976.
- [27] M. Hazas and A. Ward, "A novel broadband ultrasonic location system," in *Proc. of the International Conference on Ubiquitous Computing (UbiComp'02), Goteborg, Sweden*. Springer, 2002, pp. 264–280.
- [28] M. Hazas and A. Hopper, "Broadband ultrasonic location systems for improved indoor positioning," *IEEE Transactions on mobile Computing*, vol. 5, no. 5, pp. 536–547, 2006.
- [29] S. J. Kim and B. K. Kim, "Dynamic ultrasonic hybrid localization system for indoor mobile robots," *IEEE Transactions on Industrial Electronics*, vol. 60, no. 10, pp. 4562–4573, 2012.
- [30] H. Godrich, A. M. Haimovich, and R. S. Blum, "Target localization accuracy gain in mimo radar-based systems," *IEEE Transactions on Information Theory*, vol. 56, no. 6, pp. 2783–2803, 2010.
- [31] M. H. AlSharif, M. Saad, M. Siala, M. Ahmed, and T. Y. Al-Naffouri, "Range estimation of a moving target using ultrasound differential zadoff-chu codes," *arXiv preprint arXiv:2102.05436*, 2021.
- [32] P.-A. Absil, R. Mahony, and R. Sepulchre, *Optimization algorithms on matrix manifolds*. Princeton University Press, 2009.
- [33] S. T. Smith, "Optimization techniques on riemannian manifolds," *Fields institute communications*, vol. 3, no. 3, pp. 113–135, 1994.
- [34] C. Liu and N. Boumal, "Simple algorithms for optimization on riemannian manifolds with constraints," *Applied Mathematics & Optimization*, pp. 1–33, 2019.
- [35] P.-A. Absil, R. Mahony, and R. Sepulchre, *Optimization Algorithms on Matrix Manifolds*. Princeton, NJ: Princeton University Press, 2008.
- [36] S. Boyd and L. Vandenberghe, *Convex Optimization*. New York, NY, USA: Cambridge University Press, 2004.
- [37] P. Wolfe, "Convergence conditions for ascent methods," *SIAM review*, vol. 11, no. 2, pp. 226–235, 1969.
- [38] H. Hendriks, "A cramer-rao type lower bound for estimators with values in a manifold," *Journal of Multivariate Analysis*, vol. 38, no. 2, pp. 245–261, 1991.
- [39] S. T. Smith, "Covariance, subspace, and intrinsic cramer/spl acute/r-rao bounds," *IEEE Transactions on Signal Processing*, vol. 53, no. 5, pp. 1610–1630, 2005.
- [40] P. Stoica and Boon Chong Ng, "On the cramer-rao bound under parametric constraints," *IEEE Signal Processing Letters*, vol. 5, no. 7, pp. 177–179, 1998.
- [41] D. Chu, "Polyphase codes with good periodic correlation properties (corresp.)," *IEEE Transactions on Information Theory*, vol. 18, no. 4, pp. 531–532, 1972.
- [42] S. M. Kay, *Fundamentals of statistical signal processing*. Prentice Hall PTR, 1993.
- [43] R. H. Byrd, J. C. Gilbert, and J. Nocedal, "A trust region method based on interior point techniques for nonlinear programming," *Mathematical programming*, vol. 89, no. 1, pp. 149–185, 2000.
- [44] R. H. Byrd, M. E. Hribar, and J. Nocedal, "An interior point algorithm for large-scale nonlinear programming," *SIAM Journal on Optimization*, vol. 9, no. 4, pp. 877–900, 1999.
- [45] R. A. Waltz, J. L. Morales, J. Nocedal, and D. Orban, "An interior algorithm for nonlinear optimization that combines line search and trust region steps," *Mathematical programming*, vol. 107, no. 3, pp. 391–408, 2006.
- [46] J. Nocedal and S. Wright, *Numerical optimization*. Springer Science & Business Media, 2006.

- [47] R. H. Byrd, R. B. Schnabel, and G. A. Shultz, "A trust region algorithm for nonlinearly constrained optimization," *SIAM Journal on Numerical Analysis*, vol. 24, no. 5, pp. 1152–1170, 1987.
- [48] N. Boumal, B. Mishra, P.-A. Absil, and R. Sepulchre, "Manopt, a Matlab toolbox for optimization on manifolds," *Journal of Machine Learning Research*, vol. 15, pp. 1455–1459, 2014. [Online]. Available: <http://www.manopt.org>